12

Computational Quantum Field Theory

12.1 Introduction

The Computational Physics Group performs basic research into classical and quantum statistical physics with special emphasis on phase transitions and critical phenomena. In the centre of interest are the physics of spin glasses, diluted magnets and other materials with quenched, random disorder, soft condensed matter physics with a focus on fluctuating paths and interfaces, biologically motivated problems such as polymer collapse/folding, adsorption and aggregation as well as related properties of proteins, and the intriguing physics of low-dimensional quantum spin systems.

The methodology is a combination of numerical and analytical techniques. The numerical tools are mainly Monte Carlo (MC) and Molecular Dynamics (MD) computer simulations, chain-growth algorithms, and exact enumeration techniques. The computational approach to theoretical physics is expected to gain more and more importance with the future advances of massively parallel computer technologies, and is likely to become the third cornerstone of physics besides experiment and analytical theory as sketched in Fig. 12.1. Already now it often helps to bridge the gap between experiments and the often necessarily approximate calculations in analytic approaches. To achieve the desired high efficiency of the numerical studies we develop new algorithms and, to guarantee the flexibility required by basic research, all computer codes are implemented by ourselves. The technical tools are Fortran, C, C++, and Python programs running under Unix or Linux operating systems and computer algebra using Maple or Mathematica. The software is developed and tested at the Institute on a cluster of PCs and workstations, where also most of the numerical analyses are performed. Currently we are also exploring the possibilities of the rapidly developing graphics card computing, that is computer simulations on general purpose graphics processing units (GPGPUs) with a very large number of cores. High-performance simulations requiring vast amounts of computer time are carried out at the Institute on quite powerful compute servers, at the parallel computers of the Saxon computing centre in Dresden, and, upon successful grant application, at the national supercomputing centres in Jülich, Stuttgart and München on parallel high-capability computers. This hierarchy of various platforms gives good training and qualification opportunities for the students, which offers promising job perspectives in many different fields for their future careers.

Our research activities are closely integrated into the Graduate School "BuildMoNa": Leipzig School of Natural Sciences – *Building with Molecules and Nano-*

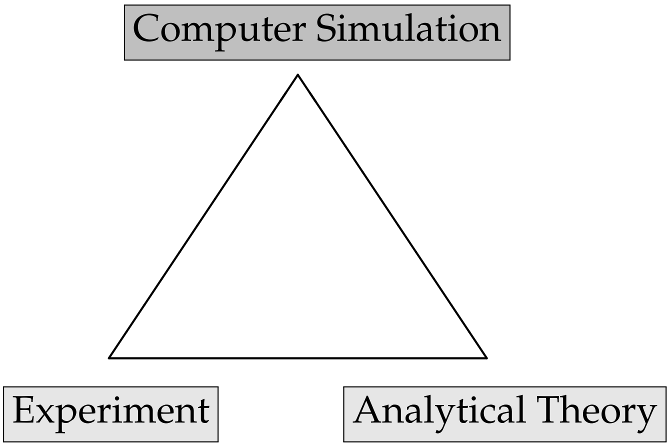

Figure 12.1: Sketch of the "triangular" relationship between experiment, analytical theory and computer simulation.

objects, the International Max Planck Research School (IMPRS) *Mathematics in the Sciences*, and the International Doctoral College *Statistical Physics of Complex Systems* with Université de Lorraine in Nancy, France, supported by the Deutsch-Französische Hochschule (DFH-UFA). In the second funding period 2011–2013, Coventry University in England has been integrated as an associated partner, and in the third funding period 2014–2016, also the National Academy of Sciences of Ukraine in Lviv has joined as another associated partner institution, offering our PhD students now several interesting options for secondments. For instance, in 2014, one PhD student started a "co-tutelle de thèse" jointly supervised with a colleague from Coventry University. Currently the DFH-UFA Doctoral College under the acronym "$\mathbb{L}^4$" is in its fourth funding period 2017–2020 and the fifth funding period 2021–2024 has recently been approved. The three Graduate Schools are all "Classes" of the Research Academy Leipzig (RALeipzig), providing the organizational frame for hosting visiting students and senior scientists, offering language courses, organizing childcare and for many other practical matters.

At a more post-graduate level our research projects are embedded into the Sonderforschungsbereich/Transregio SFB/TRR 102 *Polymers under Multiple Constraints: Restricted and Controlled Molecular Order and Mobility* together with Halle University. Our group also actively contributes to two of the top level research areas ("Profillinien") and the Centre for Theoretical Sciences (NTZ) of the University. Beside "BuildMoNa" the latter structures are particularly instrumental for our cooperations with research groups in experimental physics and biochemistry on the one hand and with mathematics and computer science on the other.

On an international scale, our research projects are carried out in a wide net of collaborations which are currently mainly funded by the Deutsch-Französische Hochschule (DFH-UFA) through the Doctoral College "$\mathbb{L}^4$" and still rooted in the recently concluded EU IRSES Network DIONICOS: *Dynamics of and in Complex Systems*, a consortium of 6 European and 12 non-European partners, including sites in Austria, England, France and Germany as well as in Armenia, Russia, Ukraine, India, the United States and Venezuela. Further close contacts and collaborations are established with research groups in Armenia, Austria, China, France, Great Britain, India, Israel, Italy, Japan, Poland, Russia, Spain, Sweden, Taiwan, Turkey, Ukraine, and the United States. These contacts are refreshed and furthered through topical Workshops, Advanced Training Modules and Tutorials, and our International Workshop series *CompPhys: New Developments in Computational Physics*, taking annually place at the end of November just before the first advent weekend.

Wolfhard Janke

12.2 Knots in semiflexible polymers

S. Majumder, M. Marenz, S. Paul, W. Janke

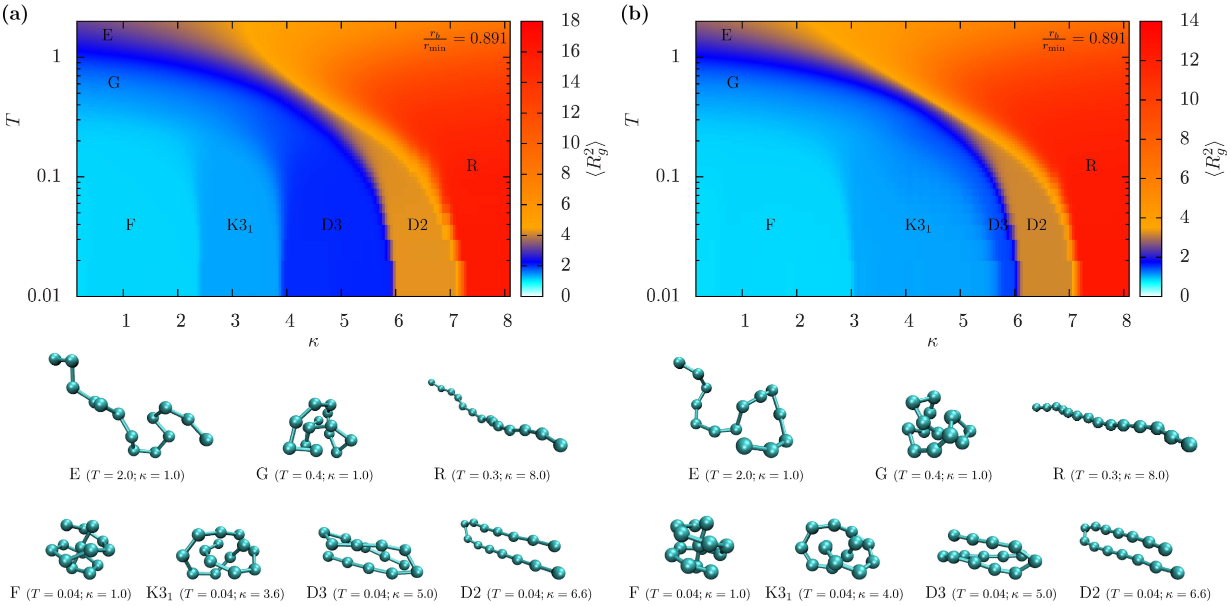

Figure 12.2: Complete phase diagram for (a) the bead-stick model and (b) the bead-spring model with the usual choice of the ratio $r_b/r_{\min} = 0.891$ for $N = 14$. The surface plots are drawn with respect to the spatial extension of the polymer chain measured in terms of the squared radius of gyration $\langle R_g^2 \rangle$. The labeled phases stand for the following: E for elongated; R for rodlike; G for globular; F for frozen; KC$_n$ for knotted phase with the corresponding knot type C_n; Dn for bent phases with n number of segments.

Knots are topological properties of closed strings, and hence, knots found in open polymers are not mathematically defined [1]. Nevertheless, by means of a special strategy for ring closure, the definition can be extended to open polymers as well [2]. Using such a protocol there have been several attempts to find knots in proteins, mostly indicating rarity of them. On the other hand, knots are more common in flexible polymers. Along the same line, even though the understanding of the phase behavior of semiflexible polymers is rich [3], there have been no reports of knotted phases until recently their presence has been identified in a bead-stick semiflexible polymers [4]. Noting the fact that the model used in Ref. [3] by Seaton *et al.* is a bead-spring model, in this study [5] we considered both a bead-spring and bead-stick model to explore the presence of any knotted phase.

We consider two semiflexible polymer models: i) bead-stick and (ii) bead-spring. In both the models the monomers are considered to be spherical beads with diameter σ, and the nonbonded interaction energy is dependent on the inter-particle distance r_{ij} and is given as

$$E_{\text{nb}} = \sum_{i=1}^{N-2} \sum_{j=i+2}^{N} \left[E_{\text{LJ}}(\min\{r_{ij}, r_c\}) - E_{\text{LJ}}(r_c)\right] \tag{12.1}$$

where

$$E_{\text{LJ}}(r_{ij}) = 4\epsilon\left[\left(\frac{\sigma}{r_{ij}}\right)^{12} - \left(\frac{\sigma}{r_{ij}}\right)^{6}\right] \tag{12.2}$$

is the standard Lennard-Jones (LJ) potential which has a minimum at $r_{\text{min}} = 2^{1/6}\sigma$. In Eq. (12.1), N is the length of the polymer measured as the total number of beads or monomers. In order to be consistent with our previous study [4] for the bead-stick model we set $\sigma = 1.0$ and do not use any cut-off in E_{nb}, whereas for the bead-spring model we choose $\sigma = 2^{-1/6}$ in order to be consistent with the choice of $r_{\text{min}} = 1.0$ in Ref. [3] and set $r_c = 2.5\sigma$ for faster computation of E_{nb}. For both models the nonbonded interaction strength ϵ is set to unity. In bead-stick models the monomers form a chain where the connectivity between successive monomers are maintained via rigid bonds having fixed length r_b. On the other hand, in a bead-spring model the bonds between successive monomers are maintained via some kind of springs. Here we consider the standard finitely extensible non-linear elastic (FENE) potential

$$E_{\text{FENE}} = -\frac{K}{2}R^2 \sum_{i=1}^{N-1} \ln\left[1 - \left(\frac{r_{ii+1} - r_b}{R}\right)^2\right] \tag{12.3}$$

where r_b is the equilibrium bond distance for which E_{FENE} is minimum. Unless otherwise mentioned in all the simulations we have used $R = 0.3$ and $K = 40$.

In both models stiffness is introduced via the well-known discretized worm-like chain cosine potential given as

$$E_{\text{bend}} = \kappa \sum_{i=1}^{N-2} (1 - \cos\theta_i) \tag{12.4}$$

where θ_i is the angle between consecutive bonds and κ controls the effective bending stiffness of the polymer. In this work we aim to perform simulations of the two models using different values of r_b/r_{min}. For that we fix the value of $r_{\text{min}} = 2^{1/6}$ and 1.0, respectively, for the bead-stick and the bead-spring model (by keeping the respective values of σ in all our simulations) and vary only the equilibrium bond length r_b. For both the models a two-dimensional replica exchange simulations were done along (T, κ) plane. The data were analysed via two-dimensional version of the weighted histogram analysis method (2D-WHAM). The knots were identified using the Alexander polynomial as described in Refs. [2] and [4].

Our results establish the fact that the presence of a stable knotted phase in the phase diagram is dependent on the ratio r_b/r_{min} where r_b is equilibrium bond length and r_{min} is the distance for strongest nonbonded contacts. Our results provide evidence for both models that if the ratio $r_b/r_{\min}$ is outside a small window around unity then depending on the bending stiffness one always encounters stable knotted phases along with the usual frozen and bent like structures at low temperatures. For an illustration see Fig. 12.2 where we show the phase diagrams of both the models for the choices of the ratio $r_b/r_{\min} = 0.891$. These findings prompt us to conclude that knots are generic stable phases in semiflexible polymers.

[1] L. Kauffman: *Knots Theory and Physics* (World Scientific, Singapore, 1991)
[2] P. Virnau: Phys. Proc. **6**, 117 (2010)
[3] D.T. Seaton et al.: Phys. Rev. Lett. **110**, 028103 (2013)
[4] M. Marenz, W. Janke: Phys. Rev. Lett. **116**, 128301 (2016)
[5] S. Majumder et al.: Macromolecules, submitted (2020)

12.3 Simulation of self-avoiding walks and polymers in continuum by means of binary trees

S. Schnabel, W. Janke

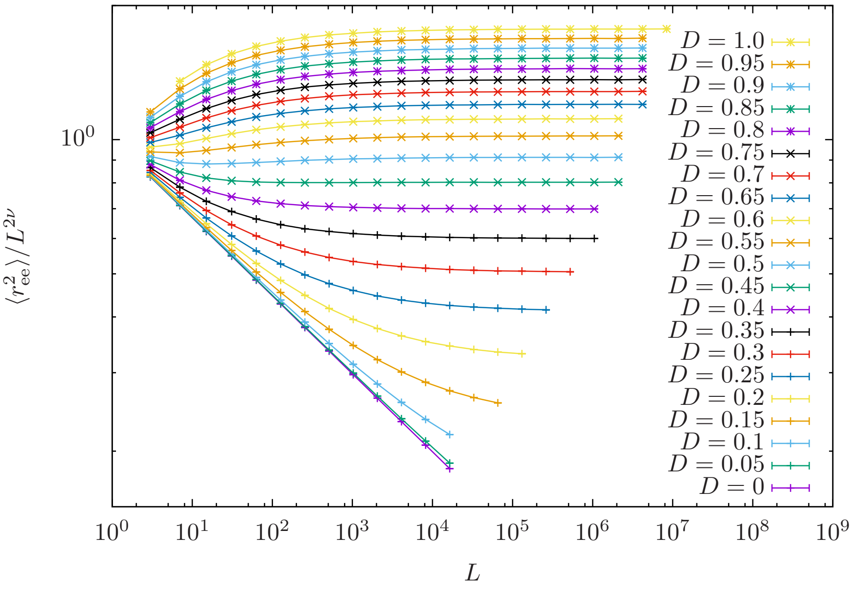

Figure 12.3: Rescaled quadratic end-to-end distance r_{ee} of the hard-sphere polymer as a function of length L for different sphere diameters D. The crossover from the random walk ($D = 0$) to the self-avoiding walk is apparent.

A few years ago Nathan Clisby has introduced a novel technique [1] for the simulation of self-avoiding walks on lattice geometries. These systems serve as simple models for polymers with excluded-volume interaction and allow for the investigation of the related scaling behaviour. With the new method walks are stored as binary trees where the leaves correspond to individual occupied lattice sites and any internal node contains collective geometric information of the subtree to which it is root in form of a box (in case of a simple-cubic lattice) that contains all derived monomers. This allows one to test for non-intersection of large parts of the walk very efficiently using nodes high up in the tree which represent many occupied lattice sites. Lower nodes representing few sites in more detail are only accessed if necessary. It was possible to determine the 3d Flory exponent with great accuracy, $\nu = 0.587\,597\,0(4)$ [2], with the new method.

Our first goal is to apply this method to the slightly more realistic hard-sphere polymer model, also known as continuum self-avoiding walks [3]. A set of monomers $\mathbf{x}_i$ that are connected by bonds of fixed length $|\mathbf{x}_i - \mathbf{x}_{i+1}| = 1$ and represent hard spheres of diameter D: $|\mathbf{x}_i - \mathbf{x}_j| \geq D$. Otherwise the chain is fully flexible. The adaptation of the binary-tree method to the latter system is straightforward. The boxes are replaced by spheres and transformations are generalized. Now it is easily possible to simulate systems with many million monomers. In Fig. 12.3 we show the dependence of the end-to-end distance as a function of the polymer length divided by the asymptotic scaling law. The crossover from a behaviour akin to a random walk (where $\nu = 1/2$) for small chains and small diameters to the self-avoiding walk (horizontal in Fig. 12.3) can be observed. It becomes apparent that for $D \approx 0.45$ the corrections to scaling become very small and asymptotic behaviour is already realized for comparatively short chains.

[1] N. Clisby: J. Stat. Phys. **140**, 349 (2010)
[2] N. Clisby, B. Dünweg: Phys. Rev. E **94**, 052102 (2016)
[3] S. Schnabel, W. Janke: Comput. Phys. Commun. **256**, 107414 (2020)

12.4 Simulation of long polymers near the Θ-point

S. Schnabel, W. Janke

The influence of the solvent on the shape of a polymer is qualitatively well understood: In a good solvent excluded volume interaction dominates and causes the polymer to arrange in an extended configuration that resembles a self-avoiding random walk, while in a bad solvent due to a high surface tension the contact area between solvent and polymer is reduced leading to a dense globular configuration. In between those two cases at the so-called Θ-point both effects cancel and the occupied configurations have the properties of an ideal Gaussian random walk, see Fig. 12.4. However, the scaling behavior that is predicted by mean-field theory has so far not been confirmed. Previously, Monte Carlo studies that were intended to solve this problem have exclusively been using lattice models, were polymer configurations are restricted to walks on (typically) cubic lattices. Although this breaks isotropy, it allows to treat much longer chains than what was possible with off-lattice models until very recently.

In order to overcome this limitation we developed a variant [1] of the well-known Metropolis Monte Carlo algorithm that works without the exact knowledge of the change in energy but still generates the correct dynamics. For the basic framework we adopted a novel technique introduced by Clisby [2] for the simulation of self-avoiding walks on lattices. It employs binary trees with nodes that represent sections of the polymer of various sizes as single units with different degrees of resolution. This scheme can be used to efficiently estimate the interaction energy of large parts of the polymer and in combination with the new Metropolis technique allows us to simulate

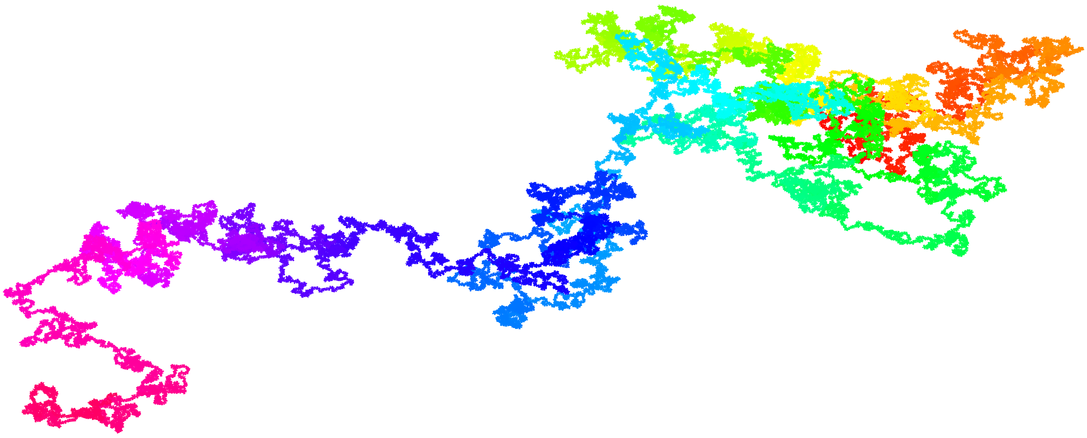

Figure 12.4: A configuration of a polymer with 65536 repeat units near the Θ-point.

large off-lattice polymers much faster. We are now able to investigate systems with more than 10^5 repeat units.

[1] S. Schnabel, W. Janke: Comput. Phys. Commun. **256**, 107414 (2020)
[2] N. Clisby: J. Stat. Phys. **140**, 349 (2010)

12.5 Computer simulations of semiflexible polymers in disordered environments

J. Bock, W. Janke

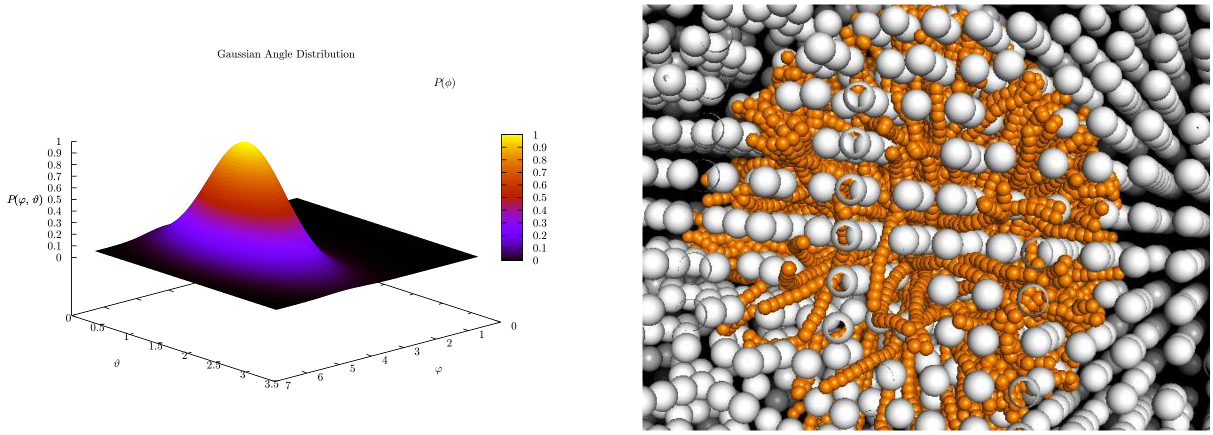

(a) Weighting histogram

(b) Semiflexible polymer in 3D disorder

Figure 12.5: (a) Histogram used for the guiding field in 3D and (b) an examplary configuration of a polymer with $N = 30$ and $\xi = 1$.

Single-molecule experiments have established the wormlike chain (WLC) as a standard model for semiflexible polymers [1]. Exploiting the analogy of the WLC with a one-

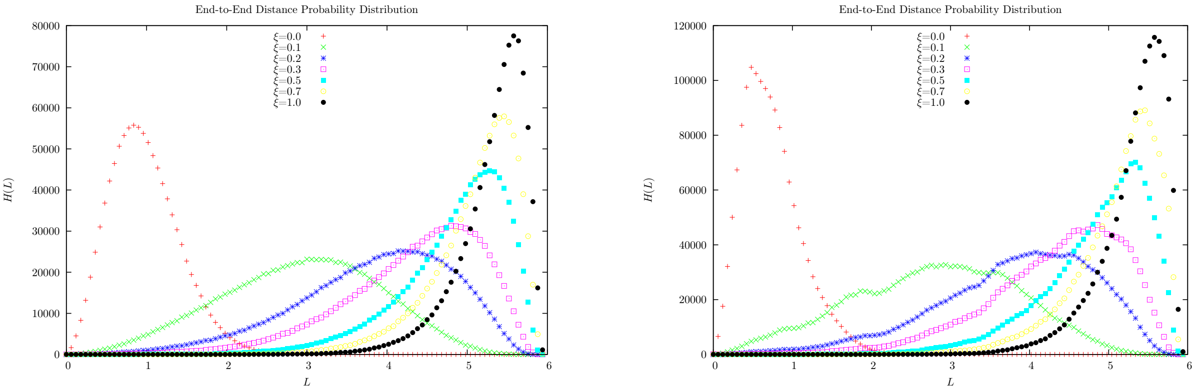

(a) Free polymers (b) Polymers in disorder

Figure 12.6: End-to-end distance distributions for (a) free polymers and (b) polymers in gaseous disorder, both in 3D.

dimensional Heisenberg ferromagnet, it can be shown that the equilibrium tangent-tangent correlation function decays exponentially. The decay rate defines the thermal persistence length l_p. When the same polymer is embedded in a quenched, disordered environment in three dimensions, this property may change quantitatively or even qualitatively. We addressed this problem by performing extensive numerical simulations of semiflexible polymers in a simple lattice disorder and in a gaseous disorder constructed by microcanonical Lennard-Jones gas simulation which represents the disordered environment. Further plans are to simulate the polymers in algebraically correlated disorder. Only the space between the spheres is accessible to the polymer. The extreme strength and density of the environmental constraints are a great challenge to conventional Monte Carlo simulation schemes, which we found hard to overcome even with a sophisticated multicanonical histogram reweighting procedure [2]. We have therefore adopted a breadth-first chain-growth algorithm [3] that resolves this difficulty by circumventing energy barriers instead of trying to cross them [2, 4], see examples in Fig. 12.5. Therefore the already existing procedures were expanded to the third dimension to investigate the behaviour of the tangent-tangent correlation length, the mean square end-to-end distance and the end-to-end probability distribution function, see Fig. 12.6. A difference in behaviour is clear and the task now is to check wether the differences scale similarly as in two dimensions, where the disorder renormalization is stated to be [5]:

$$\frac{1}{l_p^*} = \frac{1}{l_p} + \frac{1}{l_p^D},$$

with l_p^* the renormalized persistence length, l_p the persistence length given as simulation parameter and l_p^D the measured disorder persistence length.

[1] O. Otto et al.: Nat. Commun. **4**, 1780 (2013)
[2] S. Schöbl et al.: Phys. Rev. E **84**, 051805 (2011)
[3] T. Garel, H. Orland: J. Phys. A: Math. Gen. **23**, L621 (1999)
[4] S. Schöbl et al.: J. Phys. A: Math. Theor. **45**, 475002 (2012)
[5] S. Schöbl et al.: Phys. Rev. Lett. **113**, 238302 (2014)

12.6 Effect of temperature on the scaling laws governing the kinetics of collapse of a homopolymer

S. Majumder, J. Zierenberg*, W. Janke

*Max Planck Institute for Dynamics and Self-Organization, Am Fassberg 17,
37077 Göttingen, Germany

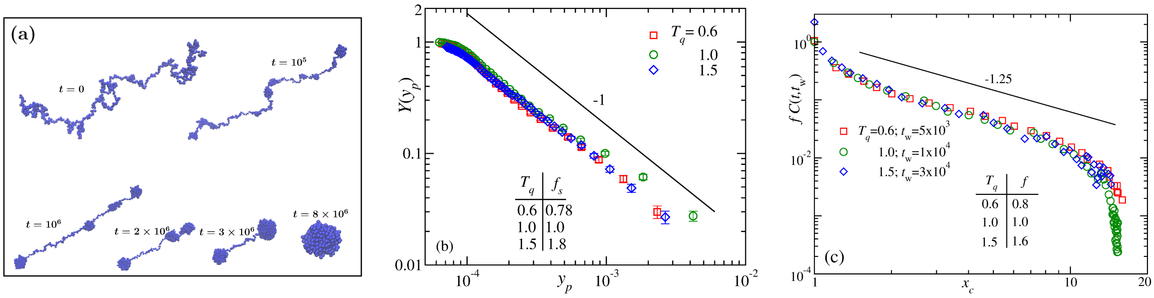

Figure 12.7: (a) Snapshots [1] showing the sequence of events occurring during the collapse of a polymer upon being quenched from an expanded state (at high temperature) into the globular phase (at low temperatures). (b) Universal finite-size scaling function $Y(y_p)$ with a non-universal metric factor f_s in the scaling variable y_p describing the scaling in the cluster growth during the collapse [2]. (c) Temperature-independent scaling plot for the aging and related dynamical scaling, probed by the behavior of a suitable density-density autocorrelation function $C(t, t_w)$ against $x_c = C_s(t)/C_s(t_w)$, the ratio of cluster sizes $C_s(t)$ at the observation time t and the waiting time t_w [2].

The collapse transition of a polymer upon transfer from a good solvent (high temperature) to a poor solvent (low temperature) bears significant connection to the folding process of a proteins and other biomolecules. Thus understanding the kinetics of a homopolymer in that respect may provide useful primary information on the underlying mechanism of more realistic problems [1, 2]. On the other hand, if one considers the usual "pear-necklace" like picture of the collpase [3] as shown in Fig. 12.7(a), it also resembles coarsening phenomena popular in spin and particle systems [4]. Over the last two years we have been exploiting this connection to understand the kinetics of collapse of a homopolymer [5].

In this work, from the state of the art Monte Carlo simulations of an off-lattice polymer model, we understand the effect of the quench temperature (T_q) on the various scaling laws related to the collapse viz., scaling of the cluster growth and the dynamical scaling related to the aging. Our results in conjunction with a nonequilibrium finite-size scaling analysis [6] show that the cluster growth is rather universal in nature and can be described by a universal finite-size scaling function with a non-universal metric factor that depends on the amplitudes of the growth [2], see Fig. 12.7(b). This observation has recently been confirmed in a related lattice model for the polymer [7]. For a direct comparison of the lattice and off-lattice formulations, see Ref. [8]. Furthermore, as can be inspected in Fig. 12.7(c), the scaling related to the aging (which is probed by a suitable two-time density-density autocorrelation function) is also found to be independent of the quench temperature T_q. A recent comprehensive overview of these findings is given in Ref. [9].

[1] S. Majumder, W. Janke: J. Phys.: Conf. Ser. **750**, 012020 (2016)
[2] S. Majumder et al.: Soft Matter **13**, 1276 (2017)
[3] A. Halperin, P. Goldbart: Phys. Rev. E **61**, 565 (2000)
[4] A.J. Bray: Adv. Phys. **51**, 481 (2002)
[5] S. Majumder, W. Janke: Europhys. Lett. **110**, 58001 (2015); Phys. Rev. E **93**, 032506 (2016)
[6] S. Majumder, S.K. Das: Phys. Rev. E **81**, 050102(R) (2010); Phys. Rev. E **84**, 021110 (2011)
[7] H. Christiansen et al.: J. Chem. Phys. **147**, 094902 (2017)
[8] S. Majumder et al.: J. Phys.: Conf. Ser. **955**, 012008 (2018)
[9] S. Majumder et al.: Eur. Phys. J. B **93**, 142 (2020)

12.7 Coarsening and aging of lattice polymers: Influence of bond fluctuations

H. Christiansen, S. Majumder, W. Janke

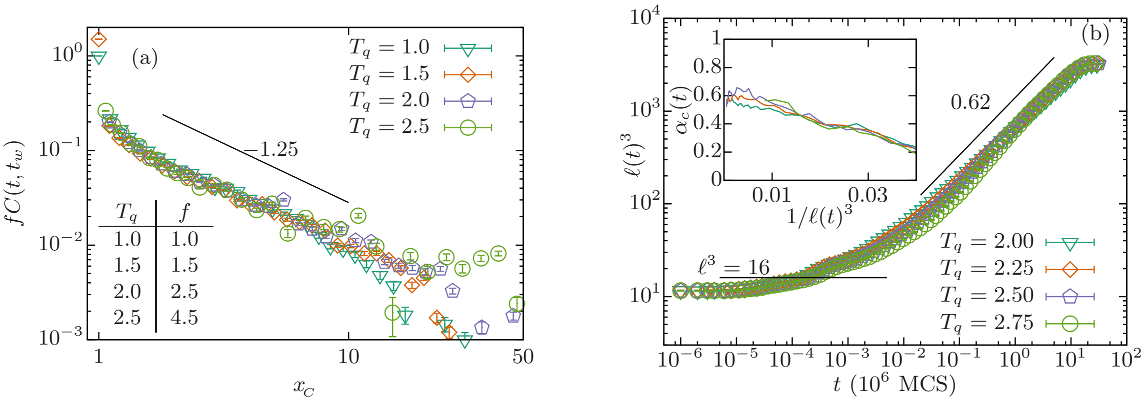

Figure 12.8: (a) The two-time correlation function $C(t, t_w)$ against the ratio of length-scales $x_C = \ell(t)/\ell(t_w)$ for the model with fixed bonds and different quench-temperatures T_q. In (b) the growth of the length-scales for the model with flexible bonds is shown for different T_q. Here the growth is independent of T_q and follows a power law with exponent $\alpha = 0.62(5)$.

The nonequilibrium properties of homopolymer collapse were investigated using Monte Carlo simulations of the interacting self-avoiding walk on a simple cubic lattice (with lattice-spacing 1) using fixed bond lengths 1 and flexible bond lengths; 1, $\sqrt{2}$, and $\sqrt{3}$ [1]. The phenomenological picture of pearl necklace polymer collapse [2] was observed, in which a polymer, when transferred from a good solvent ($T_h > T_\theta$) to a bad solvent ($T_q < T_\theta$), undergoes a collapse transition from an expanded coil by forming clusters at locally higher densities which then subsequently coalesce with each other until only a single globular cluster is left. The aging exponent $\lambda \approx 1.25$ was found to be independent of the bond conditions and the same as in the off-lattice exponent [3] [see Fig. 12.8(a) for the model with fixed bonds at different quench temperatures T_q]. For the model with flexible bonds, the power-law growth exponent of the clusters of monomers was likewise observed to be independent of temperature $\alpha = 0.62(5)$ [see Fig. 12.8(b)], while the same exponent was found to be dependent on the temperature in the fixed bond model. In the off-lattice model on the other hand, $\alpha = 1$ was found [4]. The discrepency in the exponent α is attributed to the constraints introduced by the lattice structure. For a recent review, see Ref. [5].

[1] H. Christiansen et al.: J. Chem. Phys. **147**, 094902 (2017)
[2] A. Halperin, P. M. Goldbart: Phys. Rev. E **61**, 565 (2000)
[3] S. Majumder, W. Janke: Phys. Rev. E **93**, 032506 (2016)
[4] S. Majumder, W. Janke: Europhys. Lett. **110**, 58001 (2015)
[5] S. Majumder et al.: Eur. Phys. J. B **93**, 142 (2020)

12.8 Scaling laws during collapse of a homopolymer: Lattice versus off-lattice

S. Majumder, H. Christiansen, W. Janke

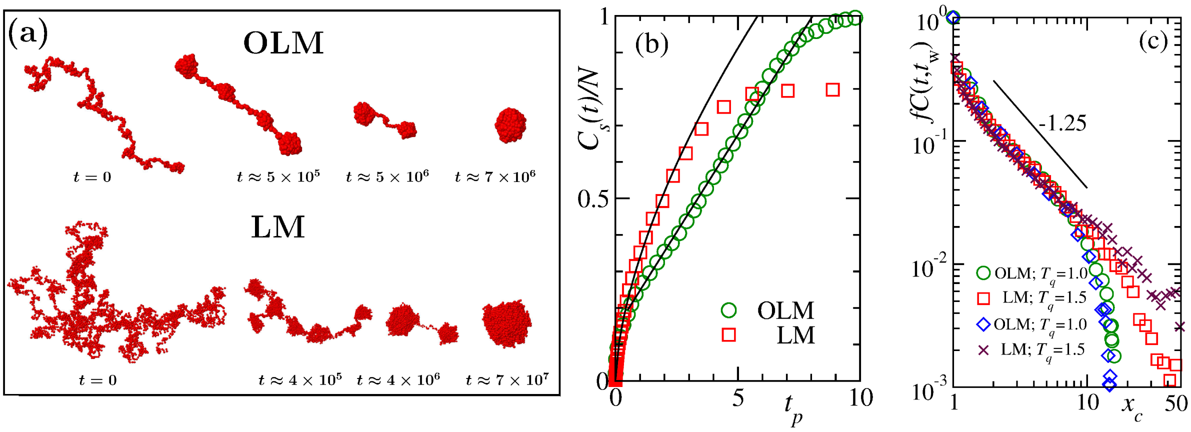

Figure 12.9: (a) Time evolution snapshots of the collapse of a homopolymer, after being quenched from an extended coil phase to a temperature, $T_q = 1$ for OLM, and $T_q = 2.5$ for LM, in the globular phase.(b) Plots of the average cluster size $C_s(t)/N$ as function of time for the two models. To make both the data visible on the same plot, we divide the time axis by a factor m to obtain $t_p = t/m$, where $m = 1 \times 10^6$ and 3.5×10^6, respectively, for OLM and LM. The solid lines there are fits to the form $C_s(t) = C_0 + At^{\alpha_c}$ with $\alpha_c = 0.98$ for OLM and $\alpha_c = 0.62$ for LM. (c) Plot showing that universal aging scaling at different T_q for the two models can be described by a single master-curve behavior. The solid line here also corresponds to $C(t, t_w) = A_C x_c^{-\lambda_C}$ with $\lambda_C = 1.25$. Note that $C(t, t_w)$ is multiplied by a factor f to make them collapse onto the same curve. For OLM $t_w = 10^4$ whereas for LM $t_w = 10^3$.

The pathways of collapse of a homopolymer, upon a transfer from a good to a poor solvent, bears resemblance to coarsening processes. Simulation results in this context can be explained by the phenomenonlogical "pearl-necklace" picture of Halperin and Goldbart (HG) [1]. Recently we have shown via Monte Carlo simulations of both a lattice model (LM) and an off-lattice model (OLM) polymer that this nonequilibrium evolution dynamics is also a scaling phenomenon [2]. In this work we compared the results obtained from the LM and OLM, in particular the scaling of the cluster growth [3] and the aging scaling [4] probed by the two-time density-density autocorrelation function.

For the OLM, we opt for the bead-spring model of a flexible homopolymer in $d = 3$ dimensions where bonds between successive monomers are maintained via the standard finitely extensible non-linear elastic (FENE) potential

$$E_{\mathrm{FENE}}(r_{ii+1}) = -\frac{KR^2}{2}\ln\left[1-\left(\frac{r_{ii+1}-r_0}{R}\right)^2\right], \tag{12.5}$$

with $K = 40$, $r_0 = 0.7$ and $R = 0.3$. The nonbonded interaction energy is modeled by $E_{\mathrm{nb}}(r_{ij}) = E_{\mathrm{LJ}}(\min(r_{ij}, r_c)) - E_{\mathrm{LJ}}(r_c)$, where

$$E_{\mathrm{LJ}}(r) = 4\epsilon\left[\left(\frac{\sigma}{r}\right)^{12} - \left(\frac{\sigma}{r}\right)^{6}\right] \tag{12.6}$$

is the standard Lennard-Jones (LJ) potential with $\sigma = r_0/2^{1/6}$ as the diameter of the monomers, ϵ (= 1) as the interaction strength and $r_c = 2.5\sigma$ as the cut-off radius.

For LM, we consider [5] a variant of the interactive self-avoiding walk on a simple-cubic lattice, where each lattice site can be occupied by a single monomer. The energy is given by

$$E_{\mathrm{LM}} = -\frac{1}{2}\sum_{i\neq j,j\pm1} w(r_{ij}), \quad \text{where} \quad w(r_{ij}) = \begin{cases} J & r_{ij} = 1 \\ 0 & \text{else} \end{cases}. \tag{12.7}$$

In Eq. (12.7), r_{ij} is the Euclidean distance between two nonbonded monomers i and j, $w(r_{ij})$ is an interaction parameter that considers only nearest neighbors, and $J(= 1)$ is the interaction strength. We allow a fluctuation in the bond length by considering diagonal bonds, i.e., the possible bond lengths are 1, $\sqrt{2}$, and $\sqrt{3}$.

Phenomenonlogically both LM and OLM show intermediate structures consistent with the "pear-necklace" picture of HG [Fig. 12.9(a)]. However, the cluster-growth scaling in LM and OLM are different. While the OLM yields a linear growth ($\alpha_c \approx 1$), in the LM the growth is slower ($\alpha_c \approx 0.62$) [Fig. 12.9(b)], which could be attributed to the topological constraints one experiences in a lattice model. On the other hand, surprisingly, both the models show evidence of simple aging scaling having the same autocorrelation exponent $\lambda_C \approx 1.25$ [Fig. 12.9(c)], thus implying that the aging scaling is rather universal. This allowed us to demonstrate that scaling of the autocorrelation functions for the two models can be described by a single master curve. For a more detailed discussion, see the recent review in Ref. [6]

[1] A. Halperin, P. M. Goldbart: Phys. Rev. E **61**, 565 (2000)
[2] S. Majumder et al.: J. Phys.: Conf. Ser. **955**, 012008 (2018)
[3] S. Majumder, W. Janke: Europhys. Lett. **110**, 58001 (2015)
[4] S. Majumder, W. Janke: Phys. Rev. E **93**, 032506 (2016)
[5] H. Christiansen et al.: J. Chem. Phys. **147**, 094902 (2017)
[6] S. Majumder et al.: Eur. Phys. J. B **93**, 142 (2020)

12.9 Kinetics of the collapse of polyglycine in water

S. Majumder, U.H.E. Hansmann*, W. Janke

*Department of Chemistry and Biochemistry, University of Oklahoma,
Norman, Oklahoma 73019, USA

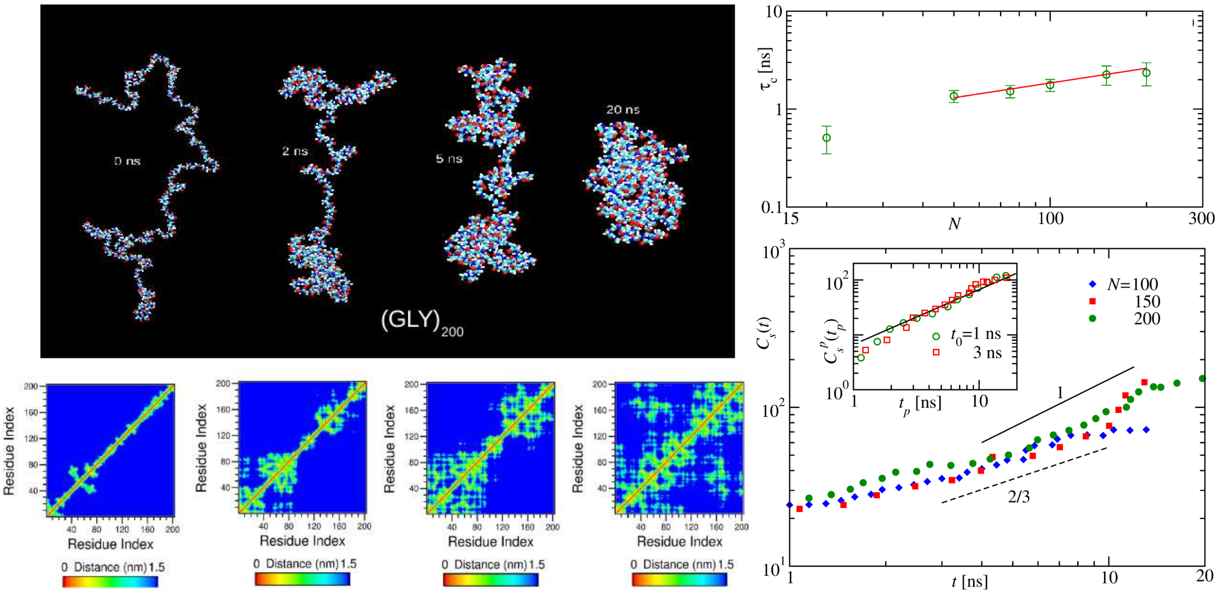

Figure 12.10: Left panel: Snapshots showing the sequence of events during collapse of polyglycine with 200 residues. Below each snapshot the corresponding contact maps are also shown revealing the pearl-necklace formation more clearly. Right panel: The upper plot shows the scaling of the collapse time τ_c with respect to the chain length. The solid line demonstrates the consistency of the data with the power-law scaling with an exponent $z = 0.5$. The lower plot shows the scaling associated with the cluster coarsening from pearl-necklace to globule.

The collapse of homopolymers was first described by de Gennes' seminal "sausage" model [1], but today the phenomenological "pearl-necklace" picture by Halperin and Goldbart [2] is more commonly used, both for flexible and semiflexible polymer models. In this picture the collapse begins with nucleation of small local clusters (of monomers) leading to formation of an interconnected chain of (pseudo-)stable clusters, i.e., the "pearl-necklace" intermediate. These clusters grow by eating up the un-clustered monomers from the chain and subsequently coalesce, leading eventually to a single cluster. Finally, monomers within this final cluster rearrange to form a compact globule.

Of central interest in this context is the scaling of the collapse time τ_c with the degree of polymerization N (the number of monomers). While scaling of the form

$$\tau_c \sim N^z, \tag{12.8}$$

where z is the dynamic exponent, has been firmly established, there is no consensus on the value of z. Molecular dynamics (MD) simulations provide much smaller values ($z \approx 1$) than Monte Carlo (MC) simulations ($z \approx 2$). This difference is often explained with the presence of hydrodynamics in the MD simulations, but a value $z \approx 1$ has been reported recently also for MC simulations [4]. The "pearl-necklace" stage or the cluster-growth kinetics can be understood by monitoring the time (t) dependence of the mean cluster size $C_s(t)$, the relevant length scale. By drawing analogy with coarsening ferromagnets it has been shown that scaling of the form

$$C_s(t) \sim t^{\alpha_c} \tag{12.9}$$

with growth exponent $\alpha_c \approx 1$ holds for flexible homopolymers [3, 4].

In this work [5] we investigated the nonequilibrium pathways by which a biological homopolymer polyglycine [$(\mathrm{Gly})_N$] collapses in water with the aim of exploring the above mentioned scaling laws. For short chains, the collapse is driven by the competition between the hydration of the peptide, opposing the collapse, and the intra-peptide attractions, favoring the collapse [6]. For chains with $N > 20$, the importance of hydration effects decreases, and the kinetics of hydrogen bonds indicates that van der Waals interactions of the backbone dominate [6] and drive the collapse. The nonequilibrium intermediates seen during the collapse exhibit local ordering or clustering that is analogous to the phenomenological "pearl-necklace" picture [cf. Fig. 12.10 (left)], known to be valid for the earlier studied coarse-grained homopolymer models [2]. Using the contact probability of the Cα-atoms in the backbone, we extract a relevant dynamic length scale, i.e., cluster size, that as in simple homopolymer models grows linearly with time [4].

Especially intriguing is that the scaling of the collapse time with length of the chain indicates a faster dynamics, with a critical exponent $z = 0.5$ [cf. Fig. 12.10 (upper right)] instead of $z = 1$ that was seen in earlier homopolymer collapse studies which considered simplified models describing non-hydrogen-bonded polymers such as polyethylene and polystyrene. The smaller exponent found in this study may be connected with a mechanism that allows in amino acid based polymers a more rapid collapse than seen in non-biological homopolymers such as poly(N-isoporpylacrylamide) and polystyrene, where collapse times of ≈ 300 ms up to ≈ 350s have been reported. We conjecture that the smaller exponent z is characteristic for collapse transitions in amino acid based polymers where the presence of intra-chain hydrogen bonding immediately seeds (transient) local ordering, while in non-hydrogen-bonded polymers such ordering happens only due to diffusive motion.

The scaling of the cluster growth during the collapse is shown in Fig. 12.10 (lower right). The solid and the dashed lines represent power-law behavior, $C_s(t) \sim t^{\alpha_c}$, with $\alpha_c = 1$ and 2/3, respectively. In the inset, two different choices for a crossover time t_0 are taken into account by plotting $C_s^p(t) \equiv C_s(t) - C_s(t)_0$ vs. $t_p = t - t_0$. Here the solid line indicates a power-law behavior with exponent $\alpha_c = 1$.

[1] P.-G. de Gennes: J. Phys. Lett. **46**, 639 (1985)
[2] A. Halperin, P. Goldbart: Phys. Rev. E **61**, 565 (2000)
[3] S. Majumder, W. Janke: Europhys. Lett. **110** 58001 (2015)
[4] S. Majumder et al.: Soft Matter **13**, 1276 (2017)
[5] S. Majumder et al.: Macromolecules **52**, 5491 (2019)
[6] D. Asthagiri et al.: J. Phys. Chem. B **121**, 8078 (2017)

12.10 Effect of Vicsek-like activity on the collapse dynamics of a flexible polymer

S. Paul, S. Majumder, S.K. Das*, W. Janke

*Theoretical Sciences Unit, Jawaharlal Nehru Centre for Advanced Scientific Research,
Jakkur P.O., Bangalore 560064, India

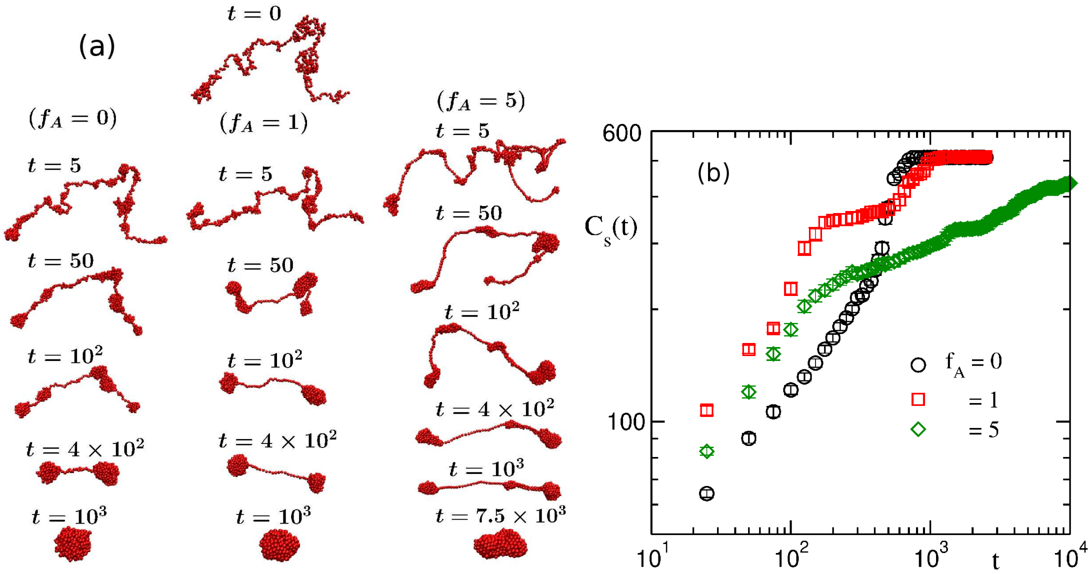

Figure 12.11: (a) Time evolution snapshots of the events occurring during the collapse transition of a polymer with $N_b = 512$ beads when quenched from an extended coil state into the globular phase at low temperature. $f_A = 0$ stands for the passive case, while $f_A = 1$ and 5 correspond to the case of an active polymer. (b) Average size of clusters as a function of time for the three cases.

A polymer undergoes a collapse transition when it is quenched from a high-temperature extended coil state (or in good solvent) to a temperature lower (or in poor solvent) than its θ-transition value, for which the equilibrium phase is a globular one. Whereas various aspects of equilibrium and nonequilibrium dynamics of such transition is reasonably well understood for the case of a passive polymer [1, 2], studies with active polymers are relatively new [3, 4]. Studying the motion of a single flexible polymer in presence of controlled active forces is necessary in case of drug delivery, directed self assembly, etc. Experimental realizations of such a system are given by linking artificially synthesized colloidal particles that show controlled motion and enhanced diffusion [5]. Here we have modeled each bead as an active element for which we applied Vicsek-like alignment interaction rules [6]. Our main aim is to look at the nonequilibrium dynamics, such as, relaxation time of collapse, cluster growth, etc. by tuning the activity and to compare them with the case of a passive polymer.

Here we consider a flexible bead-spring model of a polymer chain with N_b beads, determining the degree of polymerization [1]. The equation of motion of each bead is solved via molecular dynamics simulation using the Langevin thermostat, in which the quenching temperature has been chosen as $T = 0.5$. The interaction potentials acting among the beads consist of two terms. The non-bonded interaction is the standard LJ potential and the bonded interaction between two monomers is the FENE potential. As we have applied Vicsek-like alignment interaction rule [6], the velocity of each bead gets modified by the average direction of its neighbors present within a cut-off distance r_c, for which we choose $r_c = 2.5\sigma$, where σ is the diameter of each bead. Following Ref. [7], the active force $\vec{f_i}$ for the i'th bead can be written as,

$$\vec{f_i} = f_A \vec{D}_n \,, \tag{12.10}$$

where f_A determines the strength of the active force and $\vec{D}_n$ is the average direction determined by the neighbors.

In Fig. 12.11(a) we present comparative snapshots for a chain with $N_b = 512$ beads during the collapse of the polymer for the passive case as well for two different values of the active force [8]. Whereas the intermediate snapshots look quite different in the higher activity case ($f_A = 5$) than in the passive or $f_A = 1$ case, the final state is in all cases a globular phase. However, for $f_A = 0, 1$ the polymer evolves to a rather compact spherical globule, while for $f_A = 5$ it remains in a slightly elongated or sausage-like globular phase. And the time scale required to reach the final state is much higher for $f_A = 5$ than in the other two cases. The run time for $f_A = 5$ is up to $t = 10^4$ measured in units of LJ time scale. Though the preferred final phase is a globular one because of the presence of an attractive potential among the beads, a few realizations still remain in a dumbbell phase for $f_A = 5$. The persistance of this dumbbell phase for $f_A = 5$ increases with the value of N_b as well. To make a quantitative comparison, here in Fig. 12.11(b) we plot the average cluster size $C_s(t)$ of the clusters as a function of time for all the three cases. We see that for the active cases, though initially the growth amplitude is higher than in the passive case suggesting a faster initialization of the coarsening process, at later time $C_s(t)$ crosses over to a lower amplitude as well as a smaller exponent for the growth. This lowering of the exponent for the active case compared to the passive one is more prominent for $f_A = 5$. We will investigate these issues in more detail.

[1] S. Majumder, W. Janke: Europhys. Lett. **110**, 58001 (2015)
[2] A. Halperin, P. Goldbart: Phys. Rev. E **61**, 565 (2000)
[3] R.E. Isele-Holder et al.: Soft Matter **11**, 7181 (2015)
[4] V. Bianco et al.: Phys. Rev. Lett. **121**, 217802 (2018)
[5] B. Biswas et al.: ACS Nano **11**, 10025 (2017)
[6] T. Vicsek et al.: Phys. Rev. Lett. **75**, 1226 (1995)
[7] S.K. Das: J. Chem. Phys. **146**, 044902 (2017)
[8] S. Paul et al.: Leipzig preprint (2020)

12.11 Explicit solvent model for polymer dynamics using Lowe-Andersen approach

S. Majumder, H. Christiansen, W. Janke

Dynamics of a polymer chain in a dilute solution, although being extensively studied, is still a topic of utmost importance. In particular, this topic serves as a benchmark

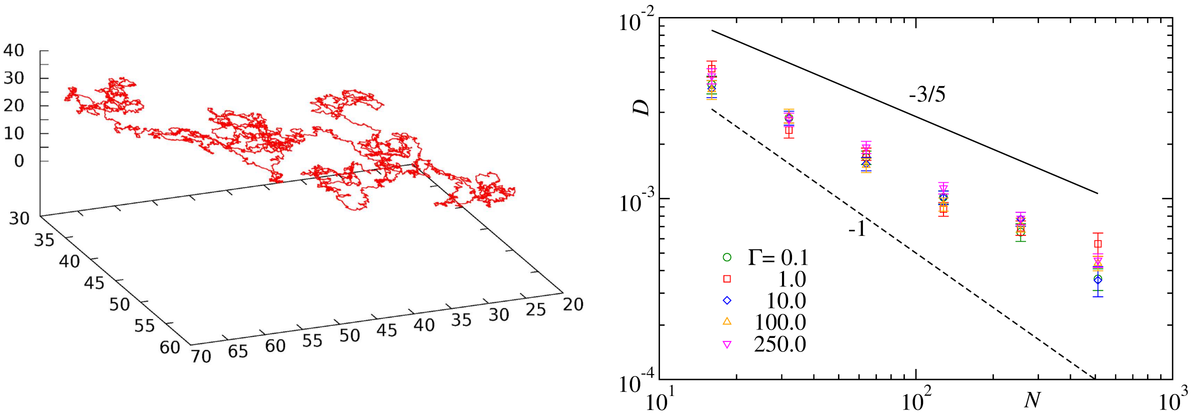

Figure 12.12: Left panel: The trajectory of the center of mass of a polymer of length $N = 512$, over a time period of 200τ in equilibrium at $T = 1.0$. Right panel: Dependence of the self-diffusion coefficient D on the chain length N of a polymer for different solvents with a collision frequency Γ as indicated. The solid and dashed lines represent the Zimm ($D \sim N^{-3/5}$) and Rouse scaling ($D \sim N^{-1}$), respectively.

for establishing a coarse-grained or mesoscopic approach to understand more realistic problems on larger time and length scales. The equilibrium dynamics of a single chain, generally, is characterized by the self-diffusion coefficient D which scales with chain length N as $D \sim N^{-x}$. In absence of hydrodynamic effects, one has $x = 1$, whereas in presence of hydrodynamic effects, one expects $x = 3/5$. The former is referred to as Rouse scaling [1] and the latter as Zimm scaling [2].

In this work [3] we construct an explicit solvent model for a polymer by considering a bead-spring model of a flexible homopolymer in three spatial dimensions. The bonds between successive monomers are maintained via the standard finitely extensible non-linear elastic (FENE) potential

$$E_{\mathrm{FENE}}(r_{ii+1}) = -\frac{K}{2}R^2 \ln\left[1 - \left(\frac{r_{ii+1} - r_0}{R}\right)^2\right] , \tag{12.11}$$

with $K = 40$, $r_0 = 0.7$ and $R = 0.3$. The monomers and the solvent molecules both are considered to be spherical beads of mass $m = 1$ and diameter σ. All nonbonded interactions are modeled by

$$E_{\mathrm{nb}}(r_{ij}) = E_{\mathrm{LJ}}\left[\min(r_{ij}, r_c)\right] - E_{\mathrm{LJ}}(r_c) , \tag{12.12}$$

where $E_{\mathrm{LJ}}(r)$ is the standard Lennard-Jones (LJ) potential given as

$$E_{\mathrm{LJ}}(r) = 4\epsilon\left[\left(\frac{\sigma}{r}\right)^{12} - \left(\frac{\sigma}{r}\right)^{6}\right] \tag{12.13}$$

with $\sigma = r_0/2^{1/6}$ as the diameter of the beads, ϵ (= 1) as the interaction strength and $r_c = 2^{1/6}\sigma$ as cut-off radius that ensures a purely repulsive interaction.

We simulate our system via molecular dynamics (MD) simulations at constant temperature using the Lowe-Andersen (LA) thermostat [4]. In this approach, one updates the position $\vec{r}_i$ and velocity $\vec{v}_i$ of the i-th bead using Newton's equations as follows,

$$\frac{d\vec{r}_i}{dt} = \vec{v}_i, \quad \frac{d\vec{v}_i}{dt} = \vec{f}_i , \tag{12.14}$$

where $\vec{f_i}$ is the conservative force (originating from the bonded and nonbonded interactions) acting on the bead. For controlling the temperature with the LA thermostat, one considers a pair of particles within a certain distance R_T [4]. Then, with a probability $\Delta t \Gamma$, a bath collision is executed, after which the pair gets a new relative velocity from the Maxwellian distribution. Here, Δt is the width of the time step chosen for the updates in Eq. (12.14) and Γ determines the collision frequency. By varying R_T and Γ, one can effectively control the frictional drag or in other words the solvent viscosity. The exchange of relative velocities with the bath is only done on its component parallel to the line joining the centers of the pair of particles, thus conserving the angular momentum. Additionally, the new velocities are distributed to the chosen pair in such a way that the linear momentum is also conserved.

Via the scaling of the radius of gyration R_g with the chain length N as $R_g \sim N^{3/5}$ we confirm that our approach yields the known static critical exponent. The method conserves both the linear and angular momenta locally, thereby preserving the hydrodynamics. Thus the scaling of the self-diffusion coefficient D with chain length N (shown in the right panel of Fig. 12.12) indicates a much faster dynamics than the Rouse dynamics, and in fact is pretty consistent with Zimm scaling $D \sim N^{-3/5}$ valid in the presence of hydrodynamic effects.

[1] P.E. Rouse: J. Chem. Phys. **21**, 1272 (1953)
[2] B.H. Zimm: J. Chem. Phys. **24**, 269 (1956)
[3] S. Majumder et al.: J. Phys.: Conf. Ser. **1163**, 012072 (2019)
[4] C.P. Lowe: Europhys. Lett. **47**, 145 (1999)

12.12 Universal finite-size scaling for kinetics of phase separation in multicomponent mixtures

S. Majumder, S.K. Das*, W. Janke

*Theoretical Sciences Unit, Jawaharlal Nehru Centre for Advanced Scientific Research,
Jakkur P.O., Bangalore 560064, India

In this work [1] we have presented results for the kinetics of phase separation in multicomponent solid mixtures in space dimension $d = 2$, via Monte Carlo simulations of the q-state conserved Potts model that has the Hamiltonian [2]

$$H = -J \sum_{\langle ij \rangle} \delta_{\sigma_i,\sigma_j}; \quad \sigma_i = 1, 2, \ldots, q; \quad J > 0 \,. \tag{12.15}$$

The primary interest in our work was to quantify the domain-growth kinetics. We achieve this via the application of appropriate finite-size scaling analyses [3–5]. Like in critical phenomena [6], this technique allows one to obtain a precise estimation of the growth exponent α, without using very large systems. We observe that finite-size effects are weak, as in the Ising model [3, 4]. By considering an initial domain length [3] in the scaling ansatz, we show that one obtains the Lifshitz-Slyozov growth, for all q, from rather early time, like in the Ising case.

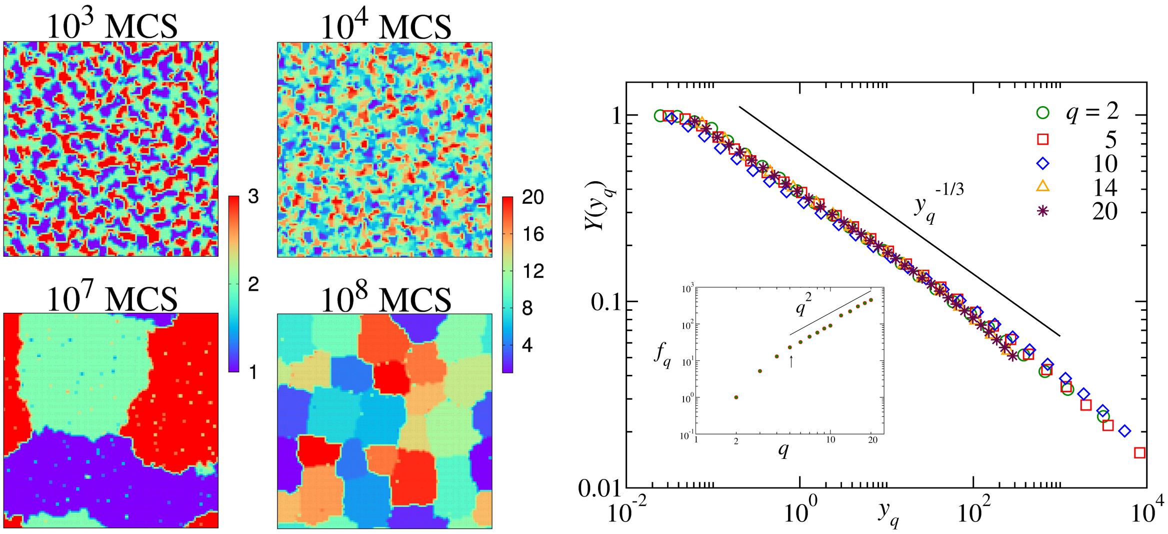

Figure 12.13: Left panel: Typical snapshots at two different times demonstrating the domain growth during phase separation in the q-state Potts model, for two different q. Results were obtained via Monte Carlo simulations mimiking diffusive dynamics. Right panel: The main frame illustrates the universality of the finite-size scaling function $Y(y_q)$ with a nonuniversal metric factor f_q in the scaling variable y_q, for different q. The inset shows the dependence of the metric factor f_q on q.

Intriguingly, we find that the growth for different q can be described by a universal finite-size scaling function $Y(y_q)$, with a nonuniversal q-dependent metric factor f_q in the scaling variable y_q, arising from the amplitude of growth. This is illustrated in the main frame of the right panel of Fig. 12.13. Similarly, for a range of quench depth, viz. $T \in [0.5T_c, 0.8T_c]$, we show that the growth follows Lifshitz-Slyozov law, irrespective of the temperature, for all q. This also can be described by a similar common finite-size scaling function. Another important fact we observed is the crossover in the behaviour of f_q as a function of q [7]. Surprisingly, this crossover happens at $q = 5$ where the nature of phase transition changes from second order to first order [2].

[1] S. Majumder et al.: Phys. Rev. E **98**, 042142 (2018)
[2] F.Y. Wu: Rev. Mod. Phys. **54**, 235 (1982)
[3] S. Majumder, S.K. Das: Phys. Rev. E **81**, 050102(R) (2010)
[4] S.K. Das et al.: Europhys. Lett. **97**, 66006 (2012)
[5] S. Majumder et al.: Soft Matter **13**, 1276 (2017)
[6] M.E. Fisher: *The theory of critical point singularities*, in *Critical Phenomena*, Proc. 51st Enrico Fermi Summer School, Varenna, Italy, edited by M.S. Green (Academic Press, London, 1971), p. 1
[7] W. Janke et al.: J. Phys.: Conf. Ser., in print (2020)

12.13 Phase-ordering kinetics of the long-range Ising model

H. Christiansen, S. Majumder, W. Janke

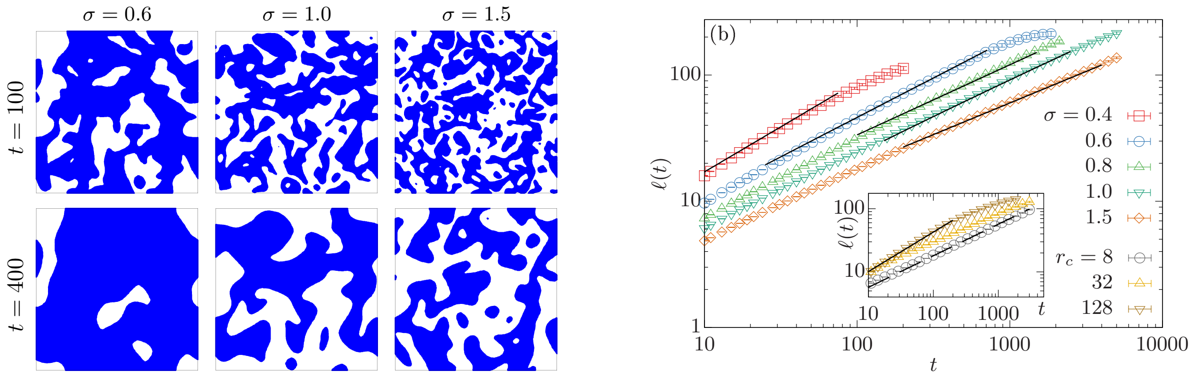

(a)

(b)

Figure 12.14: (a) Snapshots of the coarsening in the two-dimensional Ising model with long-range interactions with different $\sigma = 0.6$, 1.0, and 1.5 for the two times $t = 100$ and 400. Only spins pointing up are marked blue. (b) Length scale $\ell(t)$ for different σ, where the solid lines correspond to the prediction (12.17). The inset shows the influence of a finite cut-off on the growth of length scale.

The nonequilibrium properties of the long-range Ising model with Hamiltonian

$$\mathcal{H} = -\sum_{i}\sum_{j<i} J(r_{ij}) s_i s_j, \text{ with } J(r_{ij}) = \frac{1}{r_{ij}^{d+\sigma}} \tag{12.16}$$

are investigated. We vary the exponent σ, which controls the decay of the potential $J(r_{ij})$ between spins s_i and s_j at distance r_{ij}. In Fig. 12.14(a) we show snapshots of this system for some of those σ and for two different times. The ordering of structured regions is clearly visible, where obviously the amplitude of growth depends on σ. However, this does not tell us something about the underlying law of growth. To quantify this, we investigate the characteristic length $\ell(t)$, which we extract from the decay of the equal-time two-point spin-spin autocorrelation function. For this model, there exists a prediction [3], reading

$$\ell(t) \propto t^{\alpha} = \begin{cases} t^{\frac{1}{1+\sigma}} & \sigma < 1 \\ (t \ln t)^{\frac{1}{2}} & \sigma = 1 \\ t^{\frac{1}{2}} & \sigma > 1 \end{cases} . \tag{12.17}$$

A previous publication observed $\ell(t) \propto t^{1/2}$ independent of σ, however, using a cut-off in the potential $J(r_{i,j})$ [4]. In the inset of Fig. 12.14(b) we show the influence of the cut-off for $\ell(t)$ with $\sigma = 0.6$ and observe that one indeed finds the exponent 1/2 for small cut-offs, whereas prediction (12.17) is confirmed for a sufficiently large cut-off. In the main plot of Fig. 12.14(b) we demonstrate for the first time that indeed (12.17) holds for all σ investigated when no cut-off is used.

[1] H. Christiansen et al.: Phys. Rev. E **99**, 011301(R) (2019)
[2] W. Janke et al.: J. Phys.: Conf. Ser. **1163**, 012002 (2019)
[3] A.J. Bray, A.D. Rutenberg: Phys. Rev. E **49**, R27(R) (1994)
[4] J. Gundh et al.: PloS One **10**, e0141463 (2015)

12.14 Aging in the long-range Ising model

H. Christiansen, S. Majumder, M. Henkel*†‡, W. Janke

*Laboratoire de Physique et Chimie Théoriques (CNRS UMR 7019), Université de Lorraine
Nancy, 54506 Vandoeuvre-lès-Nancy Cedex, France
†Centro de Física Teórica e Computacional, Universidade de Lisboa,
1749-016 Lisboa, Portugal
‡Max-Planck-Institut für Physik komplexer Systeme, Nöthnitzer Straße 38,
01187 Dresden, Germany

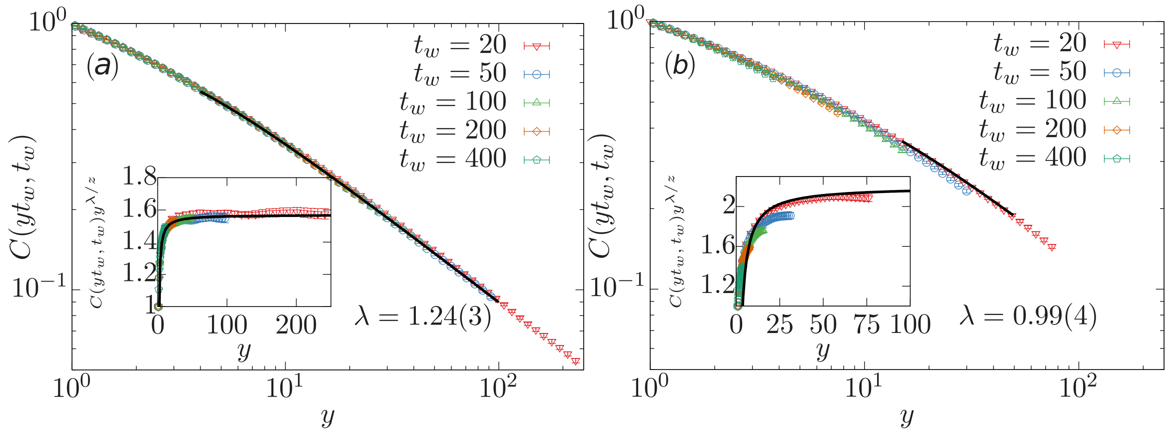

Figure 12.15: Autocorrelation function $C(t, t_w)$ versus scaling variable $y \equiv t/t_w$ for (a) $\sigma = 1.5$ and (b) $\sigma = 0.6$ for different waiting times t_w. The solid lines are fits, where the obtained autocorrelation exponent λ is mentioned in the figure. The inset shows the same data, but dividing out the asymptotic behavior, i.e., plotting $C(t, t_w)y^{\lambda/z}$ versus y.

After first having establishing the coarsening aspects of the phase-ordering kinetics of the long-range Ising model with power-law decaying interaction potential $r^{-(d+\sigma)}$ [1, 2], with the help of a clever trick in the calculation of the local energy change, we now turn our attention to the aging properties of this system [3]. The current understanding of aging phenomena is mainly confined to the study of systems with short-ranged interactions. The dynamical scaling of the two-time spin-spin autocorrelator $C(t, t_w)$ is well described by simple aging with respect to the scaling variable $y \equiv t/t_w$ for all interaction ranges σ studied. The autocorrelation exponents are quantitatively estimated and are consistent with autocorrelation exponent $\lambda = 1.25$ in the effectively short-range regime with $\sigma > 1$, while for stronger long-range interactions with $\sigma < 1$ the data are consistent with $\lambda = d/2 = 1$. This is demonstrated in Fig. 12.15, where we show in (a) for $\sigma = 1.5$ and in (b) for $\sigma = 0.6$ $C(t, t_w)$ versus y for different waiting times t_w. For all t_w, the data shows bulk behavior, whereas for big t and $\sigma = 0.6$ one observes finite-size effects. Especially for $\sigma = 0.6$ in the very long-ranged interaction regime, strong finite-size effects are observed. The solid lines are fits of form $C(t, t_w) = f_{C,\infty} t^{-\lambda/z}(1 - A/y)$, where the latter correction is justified as this is also the leading order correction term coming from exactly solvable models. We also discuss whether such finite-size effects could be misinterpreted phenomenologically as sub-aging.

[1] H. Christiansen et al.: Phys. Rev. E(R) **99**, 011301 (2019)
[2] W. Janke et al.: J. Phys.: Conf. Ser. **1163**, 012002 (2019)
[3] H. Christiansen et al.: Phys. Rev. Lett. **125**, 180601 (2020)

12.15 Percolation on square lattices with long-range correlated defects

J. Zierenberg*, N. Fricke, M. Marenz, F.P. Spitzner, V. Blavatska†, W. Janke

*Max Planck Institute for Dynamics and Self-Organization, Am Fassberg 17, 37077 Göttingen, Germany
†Institute for Condensed Matter Physics of the National Academy of Sciences of Ukraine, 79011 Lviv, Ukraine

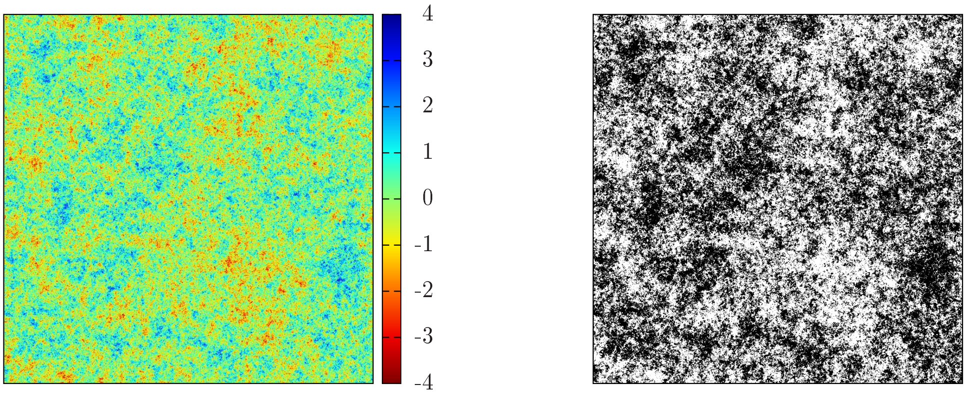

(a) (b)

Figure 12.16: Correlated continuous variables on a $2^{11} \times 2^{11}$ lattice for (a) correlation strength $a = 0.5$ and (b) corresponding discrete lattice at the percolation threshold with defects shown in black.

Structural obstacles (impurities) play an important role for a wide range of physical processes as most substrates and surfaces in nature are rough and inhomogeneous [1]. For example, the properties of magnetic crystals are often altered by the presence of extended defects in the form of linear dislocations or regions of different phases. Another important class of such disordered media are porous materials, which often exhibit large spatial inhomogeneities of a fractal nature. Such fractal disorder affects a medium's conductivity, and diffusive transport can become anomalous [2] This aspect is relevant, for instance, for the recovery of oil through porous rocks [3], for the dynamics of fluids in disordered media [4], or for our understanding of transport processes in biological cells [5].

In nature, inhomogeneities are often not distributed completely at random but tend to be correlated over large distances. To understand the impact of this, it is useful to consider the limiting case where correlations asymptotically decay by a power law rather than exponentially with distance:

$$C(r) \sim |r|^{-a} \tag{12.18}$$

where a is the correlation parameter. If a is smaller than the spatial dimension D, the correlations are considered long-range or “infinite.” An illustration of such power-law correlations for continuous and discrete site variables on a square lattice is shown in Fig. 12.16.

In this project we studied long-range power-law correlated disorder on square and cubic lattices [6, 7]. In particular, we obtained high-precision results for the percolation thresholds and the fractal dimension of the largest clusters as a function of correlation parameter a. The correlations are generated using a discrete version of the Fourier filtering method [8]. We consider two different metrics to set the length scales over which the correlations decay, showing that the percolation thresholds are highly sensitive to such system details. By contrast, we verify that the fractal dimension d_f is a universal quantity and unaffected by the choice of metric. We also show that for weak correlations, its value coincides with that for the uncorrelated system. In two dimensions we observe a clear increase of the fractal dimension with increasing correlation strength, approaching $d_f \to 2$. The onset of this change, however, does not seem to be determined by the extended Harris criterion.

As a follow-up project that heavily relies on these results, we are currently studying the site-disordered Ising model on three-dimensional lattices with long-range correlated defects [9].

[1] D. Avnir et al.: Nature (London) **308**, 261 (1984)
[2] J.-P. Bouchaud, A. Georges: Phys. Rep. **195**, 127 (1990); I. Goychuk et al.: Phys. Rev. E **96**, 052134 (2017)
[3] M. Sahimi: *Flow and Transport in Porous Media and Fractured Rock* (VCH, Weinheim, 1995)
[4] M. Spanner et al.: Phys. Rev. Lett. **116**, 060601 (2016)
[5] F. Höfling, T. Franosch: Rep. Prog. Phys. **76**, 046602 (2013)
[6] N. Fricke et al.: Condens. Matter Phys. **20**, 13004 (2017)
[7] J. Zierenberg et al.: Phys. Rev. E **96**, 062125 (2017)
[8] H.A. Makse et al.: Phys. Rev. E **53**, 5445 (1996)
[9] S. Kamin, W. Janke: Phys. Rev. B **102**, 174206 (2020)

12.16 Monte Carlo study of the Ising model in three dimensions with long-range correlated site disorder

S. Kazmin, W. Janke

We study the critical behavior of the Ising model with long-range correlated site disorder on the lattice with Monte Carlo simulation techniques. In nature the disorder often comes with a certain structure and not at random. We want to mimic this fact by introducing spatially correlated defects on the lattice. The studied Ising model with site disorder on a lattice is described by the following Hamiltonian

$$\mathcal{H} = -J \sum_{\langle xy \rangle} \eta_x \eta_y s_x s_y - h \sum_{x} \eta_x s_x \; , \tag{12.19}$$

where J is the coupling constant, $s_x = \pm 1$ is a spin at site x, $\langle xy \rangle$ stands for next-neighbor indices, h is the external magnetic field and $\eta_x = 1$ when the site is occupied by a spin or $\eta_x = 0$ if it is a defect (vacant site). We can recover the pure Ising model by setting $\eta_x = 1$ for each site x. If we set $\eta_x = 0$ randomly for each disorder realization, we arrive at the uncorrelated disorder case. In the case of correlated disorder we place them randomly but in such a way that they obey a spatial correlation decay of the form

$$\langle \eta_x \eta_y \rangle \propto \frac{1}{d(x,y)^a} , \tag{12.20}$$

where d is the distance between two sites and a is the so-called correlation decay exponent. Formally, $a = \infty$ corresponds to the uncorrelated case. Finally, the mean concentration of the defects over a number of realizations is denoted by p_d.

The universality class of the three-dimensional Ising model is expected to be different for the pure system, the uncorrelated disorder system according to the Harris criterion [1] and the correlated disorder system for $a \leq d = 3$ (strong correlation) according to the extended Harris criterion [2]. The situation is sketched in Fig. 12.17.

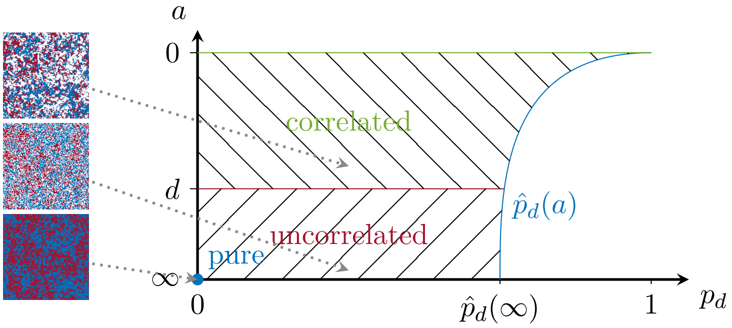

Figure 12.17: Universality classes of the three-dimensional Ising model for different disorder concentrations p_d and correlation exponents a. The curve $\hat{p}_d(a) = 1 - \hat{p}(a)$ is the percolation threshold below which the system has the probability 1 to have an infinite cluster of spins for $L \to \infty$ and therefore the Ising model is well defined. As can be seen qualitatively and was studied in Ref. [3] one can add more defects without destroying the infinite cluster of spins when the defects are correlated. On the left side slices of a three-dimensional Ising model at critical temperature are shown. White dots represent the defects $\eta_x = 0$, blue and red the spin states $s_x = \pm 1$.

We found the critical exponents of the correlation length ν and the correction exponents ω for various correlation exponents $1.5 \leq a \leq 3.5$ as well as for the uncorrelated case $a = \infty$ [4]. This was achieved by using a set of techniques such as histogram reweighting, Jackknife resampling and finite-size scaling analysis. Contrarily to other works we performed a global fit where we included up to eight different disorder concentrations $0.05 \leq p_d \leq 0.4$ into one simultaneous fit. Such a study was not possible before because most other works were limited to either only $a = 2.0$ or only one concentration of defects or even to both constraints. In Fig. 12.18 the final estimates of the critical exponents ν and ω are summarized and compared to other works. Or result for the uncorrelated case matches known results from other groups and verifies the validity of our analysis program. The correlated cases show a qualitative behavior of the form $1/a$ but deviate from the prediction $\nu = 2/a$ by about 10 %.

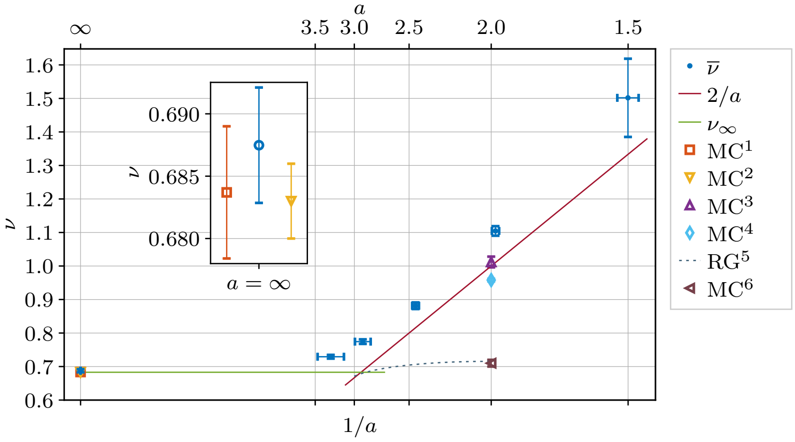

a	$\bar{\nu}$	ω
∞	0.6875(47)	0.373(53)
3.5	0.7293(56)	0.965(80)
3.0	0.7744(68)	1.008(79)
2.5	0.8814(99)	0.891(79)
2.0	1.105(15)	1.047(90)
1.5	1.50(12)	0.808(97)

Figure 12.18: Final results for the critical exponent ν compared to the known results from the literature and to the extended Harris criterion estimation $\nu = 2/a$. 1: Ballesteros et al. [5], 2: Calabrese et al. [6], 3: Ballesteros and Parisi [7], 4: Ivaneyko et al. [8], 5: Prudnikov et al. [9], 6: Prudnikov et al. [10]. The inset shows a close up of the uncorrelated case $a = \infty$. The uncorrelated case critical exponent was set to $\nu_\infty = 0.683$ as an average value from other works.

An ongoing research is to extract further critical exponents β and γ and eventually improve the current results for ν by increasing the number of disorder realizations.

[1] A.B. Harris: J. Phys. C: Solid State Phys. **7**, 1671 (1974)
[2] A. Weinrib, B.I. Halperin: Phys. Rev. B **27**, 413 (1983)
[3] J. Zierenberg et al.: Phys. Rev. E **96**, 062125 (2017)
[4] S. Kamin, W. Janke: Phys. Rev. B **102**, 174206 (2020)
[5] H.G. Ballesteros et al.: Phys. Rev. B **58**, 2740 (1998)
[6] P. Calabrese et al.: Phys. Rev. E **68**, 036136 (2003)
[7] H.G. Ballesteros, G. Parisi: Phys. Rev. B **60**, 12912 (1999)
[8] D. Ivaneyko et al.: Physica A **387**, 4497 (2008)
[9] V.V. Prudnikov et al.: Phys. Rev. B **62**, 8777 (2000)
[10] V.V. Prudnikov et al.: Condens. Matter Phys. **8**, 213 (2005)

12.17 Random field q-state Potts model: Ground states and low-energy excitations

R. Kumar*, M. Kumar†‡, M. Weigel§, V. Banerjee‡, S. Puri†, W. Janke

*Doctoral College for the Statistical Physics of Complex Systems, Leipzig-Lorraine-Lviv-Coventry ($\mathbb{L}^4$)
†School of Physical Sciences, Jawaharlal Nehru University, New Delhi – 110067, India
‡Department of Physics, Indian Institute of Technology, Hauz Khas, New Delhi – 110016, India
§Applied Mathematics Research Centre, Coventry University, England, UK

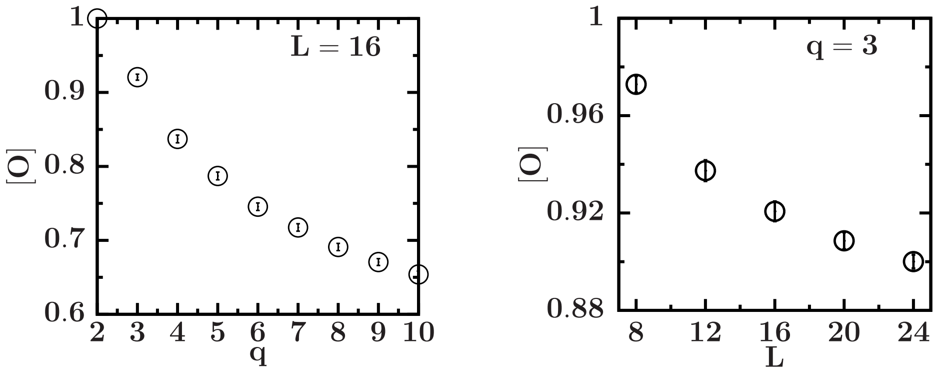

(a) (b)

Figure 12.19: Overlap between the lowest states found by graph-cut methods (GCM) and the putative ground state (a) as a function of the number of Potts states q and (b) as a function of system size L.

While the ground-state (GS) problem for the random-field Ising model is polynomial and can be solved by using a number of well-known algorithms for maximum flow [1–4], the analogue random-field q-state Potts model with $q \geq 3$ corresponds to a multi-terminal flow problem that is known to be NP hard. Hence an efficient exact algorithm is extremely unlikely to exist [5]. Still, it is possible to employ an embedding of binary degrees of freedom into the Potts spins to use graph-cut methods (GCMs) to solve the corresponding ground-state problem approximately with polynomial methods. It is shown in this project [6] that this works relatively well. We compare results produced by this heuristic algorithm to energy minima found by an appropriately tuned parallel tempering method that is configured to find ground states for the considered system sizes with high probability. The method based on graph cuts finds the same states in a fraction of the time. The new method is used for a first exploratory study of the random-field Potts model in $d = 2, 3$.

We observe that the probability of finding a ground state decreases exponentially with q for GCM, but for parallel tempering this decay is linear [Fig. 12.19(a)]. Hence, GCM is more suitable for lower q studies. We also find that the lower energies found by GCM are very close to the ground state and the excess energy is very small. The probability of finding the ground state falls exponentially with the system size, whereas for GCM it falls linearly [Fig. 12.19(b)]. Therefore, GCM is better suited for studying larger system sizes. This is one very good feature of GCM as for the smaller system sizes we have larger finite-size effects. The overlap between the states found by GCM and the ground state is observed to be very large. Hence, we conclude that GCM produces the approximate GS which can be treated as an exact GS for sufficiently small q ($q = 3, 4$) for studying the critical behaviour and ground-state morphologies.

[1] G.P. Shrivastav et al.: Europhys. Lett. **96**, 36003 (2011)
[2] G.P. Shrivastav et al.: Phys. Rev. E **90**, 032140 (2014)
[3] G.P. Shrivastav et al.: Eur. Phys. J. E **37**, 98 (2014)
[4] V. Banerjee et al.: Ind. J. Phys. **88**, 1005 (2014)
[5] J.C. Angles d'Auriac et al.: J. Physique Lett. **46**, L173 (1985)
[6] M. Kumar et al.: Phys. Rev. E **97**, 053307 (2018)

12.18 Distribution of local minima for the Edwards-Anderson spin-glass model

S. Schnabel, W. Janke

In statistical physics the term "complex behavior" is usually used to characterize systems that posses a rough free-energy landscape with many metastable states. This can be the result of competing interactions on different scales like in the case of protein folding or it may arise from quenched disorder as for spin glasses. A conceptually simple model for such a system is the Edwards-Anderson spin-glass model [1], whose Hamiltonian is given by

$$\mathcal{H} = \sum_{\langle ij \rangle} J_{ij} S_i S_j,$$

where the spins sit on the sites of a cubic lattice, can take two values $S_i \in \{-1, 1\}$, and adjacent spins interact via normally distributed random couplings J_{ij}. Since these interactions can be either ferromagnetic (positive) or antiferromagnetic (negative), there is no trivial order established at low temperatures. Instead, many very different pure states might coexist, each one of them corresponding to a minimum in free energy.

Albeit not identical, minima of the energy, i.e. spin configurations that are stable against single spin flips are closely related to these pure states. It is thought that minima in energy form the end-points of hierarchical tree-like structures with branches corresponding to different pure states. Understanding their properties might, therefore, improve our understanding of the behavior of the system. However, they have proven to be a very demanding subject of inquiry.

We have developed an advanced Monte Carlo method that in its basic form allows to sample the local energy minima with uniform distribution, i.e., each minimum configuration is occupied with equal probability [3–5]. This is achieved by establishing within the simulation the combination of a spin configuration together with a random minimization thereof. I.e., the repeated flipping of spins with positive energy until a local minimum is reached. If one now alters the spin configuration and the parameters of the minimization in a suitable way it is possible to ensure that all local minima are equally likely found this way. This corresponds to 'simple sampling' in the space of local minima. It is also possible to perform 'importance sampling' by including suitable weight functions. We can for instance sample a canonical distribution of local minima in energy by including the Boltzmann weight [6].

A basic application of this method is the measurement of the distribution of the energy minima. Since existing algorithms are unable to perform such a task, there is no numerical data for comparison. However, we can use our results to test analytical approximations [2] that are based on the expansion of meanfield solutions. We found that there are considerable deviations (Fig. 12.20) [3]. In fact, the distributions much more closely – although not entirely – resemble Gaussian distributions.

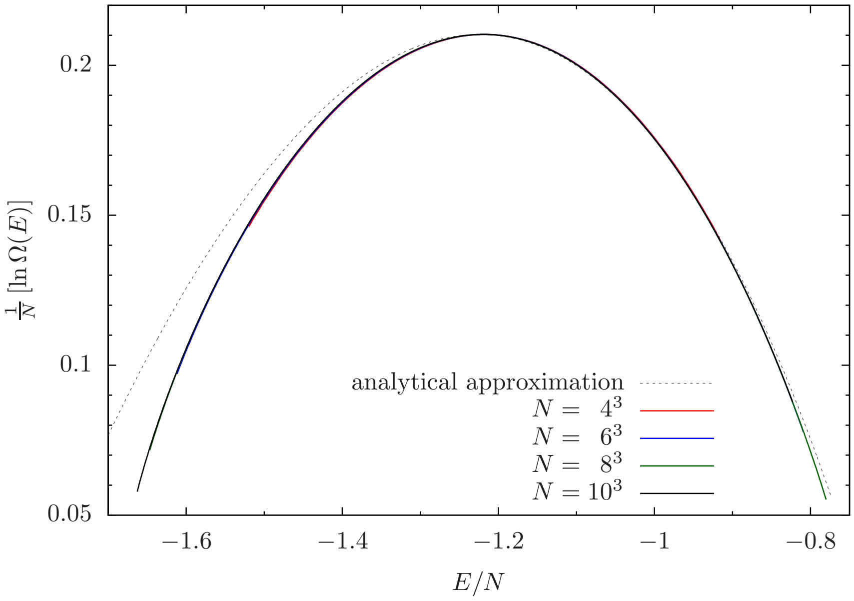

Figure 12.20: The distribution of local minima for different system sizes and the analytical approximation.

[1] S.F. Edwards, P.W. Anderson: J. Phys. F **5**, 965 (1975)
[2] A.J. Bray, M.A. Moore: J. Phys. C **14**, 1313 (1981)
[3] S. Schnabel, W. Janke: Phys. Rev. B **97**, 174204 (2018)
[4] S. Schnabel, W. Janke: J. Phys.: Conf. Ser. **1252**, 012001 (2019)
[5] S. Schnabel, W. Janke: Eur. Phys. J. B **93**, 53 (2020)
[6] S. Schnabel, W. Janke: Comput. Phys. Commun. **220**, 74 (2017)

12.19 Massively parallel simulations on GPUs for disordered systems

R. Kumar*, J. Gross, W. Janke, M. Weigel†

*Doctoral College for the Statistical Physics of Complex Systems, Leipzig-Lorraine-Lviv-Coventry ($\mathbb{L}^4$)
†Applied Mathematics Research Centre, Coventry University, England, UK

Simulations of systems with quenched disorder are extremely demanding, suffering from the combined effect of slow relaxation and the need of performing the disorder average. As a consequence, new algorithms, improved implementations, and alternative and even purpose-built hardware are often instrumental for conducting meaningful

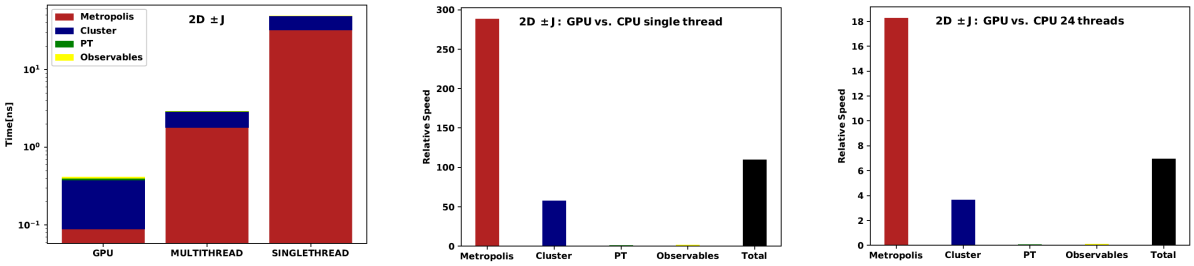

(a) (b) (c)

Figure 12.21: (a) Times spent in the different parts of the simulation on a log-scale on GPU and single-threaded as well as multi-threaded CPU implementations for 2D spin-glass systems of linear size $L = 40$ with couplings drawn from a bimodal ($\pm J$) distribution. The middle and right panels show relative timings (speed-ups) of the GPU code as compared to the (b) single-threaded and (c) multi-threaded CPU runs, respectively.

studies of such systems. Examples include our recent studies of random field Ising and Potts models [1] which motivated the present project. The ensuing demands regarding hardware availability and code complexity are substantial and sometimes prohibitive. In this study [2] we demonstrate how with a moderate coding effort leaving the overall structure of the simulation code unaltered as compared to a CPU implementation, very significant speed-ups can be achieved from a parallel code on Graphics Processing Units (GPUs) by mainly exploiting the trivial parallelism of the disorder samples and the near-trivial parallelism of the parallel tempering replicas. A combination of this massively parallel implementation with a careful choice of the temperature protocol for parallel tempering as well as efficient cluster updates allows us to equilibrate comparatively large systems with moderate computational resources.

We discuss the computational challenges of simulating disordered systems on modern hardware, and present a versatile and efficient implementation of the full spin-glass simulation stack consisting of single-spin flips, cluster updates and parallel-tempering updates in CUDA. Due to the favorable relation of performance to price and power consumption in GPUs, they have turned into a natural computational platform for the simulation of disordered systems. While a range of very efficient, but also very complex, simulational codes for the problem have been proposed before [3–6], our focus in the present work was on the provision of a basic simulation framework that nevertheless achieves a significant fraction of the peak performance of GPU devices for the simulation of spin-glass systems. A comparison of the performance achieved on GPUs and CPUs is shown in Fig. 12.21. To be representative of typical installations accessible to users, we used Nvidia GPUs from the consumer series (GTX 1080).

[1] M. Kumar et al.: Phys. Rev. E **97**, 053307 (2018)
[2] R. Kumar et al.: Eur. Phys. J. B **93**, 79 (2020)
[3] M. Bernaschi et al.: Comput. Phys. Commun. **182**, 1265 (2011)
[4] T. Yavors'kii, M.Weigel: Eur. Phys. J. Special Topics **210**, 159 (2012)
[5] M. Baity-Jesi et al.: Phys. Rev. B **89**, 014202 (2014)
[6] M. Lulli et al.: Comput. Phys. Commun. **196**, 290 (2015)

12.20 Acceptance rate is a thermodynamic function in local Monte Carlo algorithms

E. Burovski*, W. Janke, M. Guskova*, L. Shchur*†

*National Research University Higher School of Economics, 101000 Moscow, Russia
†Landau Institute for Theoretical Physics, 142432 Chernogolovka, Russia

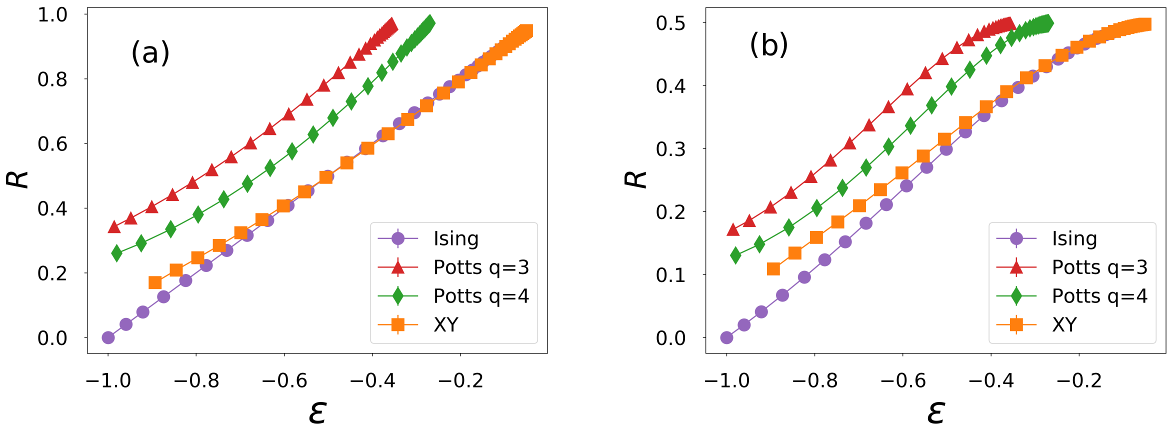

Figure 12.22: Average acceptance rates for several one-dimensional models using (a) Metropolis updates and (b) heat-bath updates.

In this study [1] we investigate properties of Markov chain Monte Carlo simulations of classical spin models with local updates. We derive analytic expressions for the mean value of the acceptance rate of single-spin-flip algorithms (Metropolis, Glauber respectively heat bath) for the one-dimensional Ising model. For the Metropolis algorithm we find that the average acceptance rate is a linear function of energy [see Fig. 12.22(a)], which moreover – and rather unexpectedly – turned out to be independent of system size.

We further provide numerical results for the energy dependence of the average acceptance rate for the 3- and 4-state Potts model, and the XY model in one and two spatial dimensions. Our results in one dimension using Matropolis respectively heat-bath updates are shown in Fig. 12.22. In all cases, the acceptance rate turns out to be an almost linear function of the energy in the critical region. The variance of the acceptance rate is studied as a function of the specific heat. While the specific heat develops a singularity in the vicinity of a phase transition, the variance of the acceptance rate stays finite.

[1] E. Burovski et al.: Phys. Rev. E **100**, 063303 (2019)

12.21 Non-flat histogram techniques for spin glasses

F. Müller, S. Schnabel, W. Janke

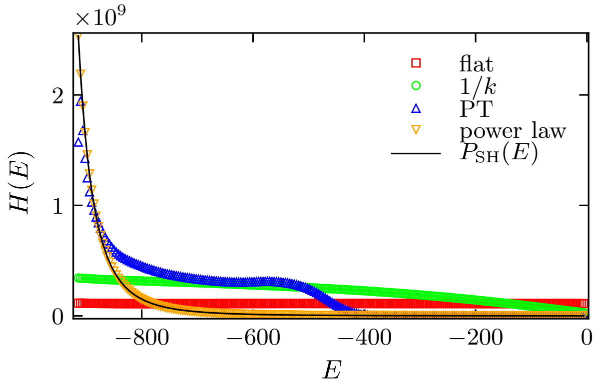

Figure 12.23: Histograms of the simulation with the different methods together with the prescribed power-law shape $P_{\mathrm{SH}}(E)$.

We took into consideration the three-dimensional bimodal Edwards-Anderson (EA) spin-glass model [1]. Spin glasses are difficult to simulate with conventional simulation methods and their investigation requires calculating disorder averages over a sufficiently large set of samples. Each sample has its own characteristics and it is known that finding the ground state of hard samples, i.e., solving the underlying optimization problem of that sample, is NP-hard.

There are existing methods such as the multicanonical (MUCA) method [2, 3], the $1/k$ ensemble [4] and parallel tempering (PT) [5] which have already been applied to the three-dimensional EA model. Especially also their performance in terms of the ability to solve the underlying optimization problem has been investigated. We looked at the round-trip times in energy which are defined as the average time which a simulation takes to reach the ground state and travel back to high energies. The ability of finding the ground state strongly influences the round-trip times of the respective method.

In addition to the above mentioned methods we modified the MUCA approach from sampling a flat distribution in energy to sampling a power-law shaped distribution in energy with a parametric form of the distribution of the form

$$P_{\mathrm{SH}}(E, \mathit{\Delta} E, \alpha) = \left(\frac{E}{\mathit{\Delta} E - E_g} + 1 \right)^{\alpha} , \tag{12.21}$$

where $\mathit{\Delta} E = 96$ is the position of the pole of the power law relative to the ground-state energy E_g and $\alpha = -3.6$ is the exponent [6]. In Fig. 12.23 the outcoming histograms of one sample with linear lattice size $L = 8$ are plotted. The figure shows clearly that the effort of the simulation is concentrated towards the ground-state region for all methods but the traditional MUCA. The power-law MUCA and PT have similar distributions of sampled states which increase drastically towards the ground-state energy.

Table 1 shows the comparison of the mean round-trip times for the three different methods. The mean round-trip times of the power-law MUCA improve significantly compared to the traditional MUCA and also compared to the other methods.

[1] S.F. Edwards, P.W. Anderson: J. Phys. F **5**, 965 (1975)
[2] B.A. Berg, T. Neuhaus: Phys. Lett. B **267**, 249 (1991); Phys. Rev. Lett. **68**, 9 (1992)
[3] W. Janke: Int. J. Mod. Phys. C **03**, 1137 (1992)

Table 12.1: Ratios of the population mean and the quantile mean of round-trip times of the flat MUCA and parallel-tempering methods with respect to the power-law MUCA method.

	flat MUCA		parallel tempering	
L	r_{pop}	$r_{\epsilon=10^{-4}}$	r_{pop}	$r_{\epsilon=10^{-4}}$
3	$1.16^{+0.02}_{-0.02}$	$1.17^{+0.04}_{-0.04}$	$1.64^{+0.03}_{-0.03}$	$1.64^{+0.04}_{-0.04}$
4	$1.62^{+0.05}_{-0.05}$	$1.66^{+0.09}_{-0.08}$	$1.17^{+0.04}_{-0.04}$	$1.22^{+0.07}_{-0.07}$
5	$2.3^{+0.2}_{-0.2}$	$2.34^{+0.3}_{-0.3}$	$1.14^{+0.05}_{-0.05}$	$1.14^{+0.1}_{-0.09}$
6	$3.8^{+0.6}_{-0.5}$	$3.5^{+0.7}_{-0.6}$	$2.8^{+0.4}_{-0.4}$	$3.3^{+0.8}_{-0.6}$
8	13^{+12}_{-7}	$15^{+25}_{-10.0}$	3^{+3}_{-2}	3^{+6}_{-2}

[4] B. Hesselbo, R.B. Stinchcombe: Phys. Rev. Lett. **74**, 2151 (1995)
[5] K. Hukushima, K. Nemoto: J. Phys. Soc. Jpn. **65**, 1604 (1996)
[6] F. Müller et al.: Phys. Rev. E **102**, 053303 (2020)

12.22 Population annealing: A massively parallel computer simulation scheme

M. Weigel[*], L.Yu. Barash[†‡], M. Borovský[§], L.N. Shchur[†‡¶], W. Janke

[*]Applied Mathematics Research Centre, Coventry University, England, UK
[†]Landau Institute for Theoretical Physics, 142432 Chernogolovka, Russia
[‡]Science Center in Chernogolovka, 142432 Chernogolovka, Russia
[§]P.J. Šafárik University, Park Angelinum 9, 040 01 Košice, Slovak Republic
[¶]National Research University Higher School of Economics, 101000 Moscow, Russia

The generic technique for Monte Carlo simulations in statistical physics is importance sampling via a suitably constructed Markov chain [1]. While such approaches are quite successful, they are not particularly well suited for parallelization as the chain dynamics is sequential, and if replicated chains are used to increase statistics each of them relaxes into equilibrium with an intrinsic time constant that cannot be reduced by parallel work. Population annealing is a sequential Monte Carlo method that simulates an ensemble of system replica under a cooling protocol as sketched in Fig. 12.24. This method was first suggested in 2001 by Iba [2] and later on discussed in more detail by Hukushima and Iba [3] as a method to tackle potentially difficult sampling problems, but with no particular view to a parallel implementation. More recently, Machta [4] used a variant that avoids the recording of weight functions through population control in every step. This is the variant we adapted in our own implementation.

The population element makes this method naturally well suited for massively parallel simulations, and both the bias in estimated quantities and the statistical errors can be systematically reduced by increasing the population size. To demonstrate this, we developed an implementation of population annealing on graphics processing units (GPUs) [5] and benchmarked its behaviour for different systems undergoing continuous and first-order phase transitions [6, 7]. For a recent overview, see Ref. [8].

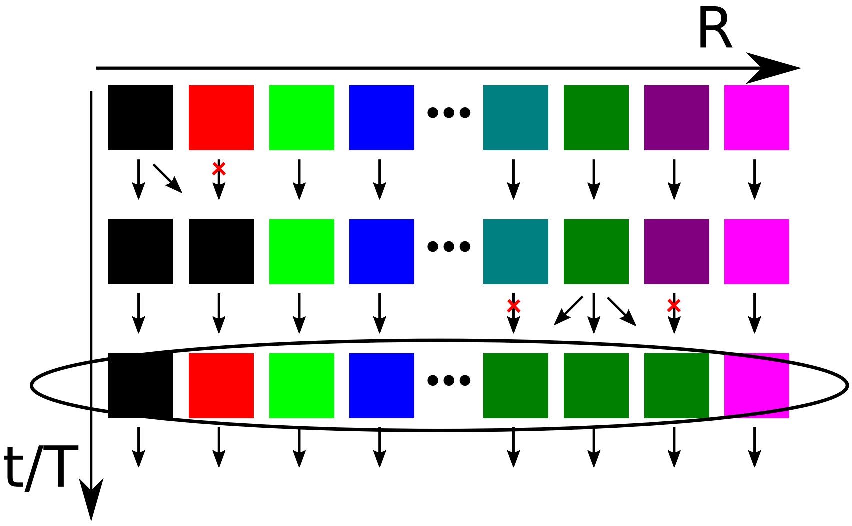

Figure 12.24: Schematic illustration of the population annealing method: R replica of the system are cooled down in discrete temperature steps. At each temperature T the current configurations at the next higher temperature are resampled according to their Boltzmann weights. This amounts to deleting some of them (e.g., the red one in the upper row) and replicating others one, two or more times (e.g., the dark green one in the second row). This new population is then further evolved in "time" t by any valid update procedure at this temperature.

[1] D.P. Landau, K. Binder: *A Guide to Monte Carlo Simulations in Statistical Physics*, 4th ed. (Cambridge University Press, Cambridge, 2015)
[2] Y. Iba: Trans. Jpn. Soc. Artif. Intell. **16**, 279 (2001)
[3] K. Hukushima, Y. Iba: AIP Conf. Proc. **690**, 200 (2003)
[4] J. Machta: Phys. Rev. E **82**, 026704 (2010)
[5] L.Yu. Barash et al.: Comput. Phys. Commun. **220**, 341 (2017)
[6] L.Yu. Barash et al.: Eur. Phys. J. – Special Topics **226**, 595 (2017)
[7] M. Weigel et al.: in *Computer Simulation Studies in Condensed-Matter Physics XXX*, eds. D.P. Landau, M. Bachmann, S.P. Lewis, H.-B. Schüttler, Phys.: Conf. Ser. **921**, 012017 (2017)
[8] L. Shchur et al.: Communications in Computer and Information Science (CCIS) **965**, 354 (2019)

12.23 Accelerating molecular dynamics with population annealing

H. Christiansen, M. Weigel*, W. Janke

*Applied Mathematics Research Centre, Coventry University, England, UK

Systems having a rugged free-energy landscape cannot be simulated using naive canonical (NVT) simulations, because they get trapped in local minima. Therefore, one uses so-called generalized ensemble methods to overcome those barriers. In Molecular Dynamics, one mostly uses Parallel Tempering [1], which is easy to parallelize. However, this method can only effectively use a limited number of CPU cores. In this work,

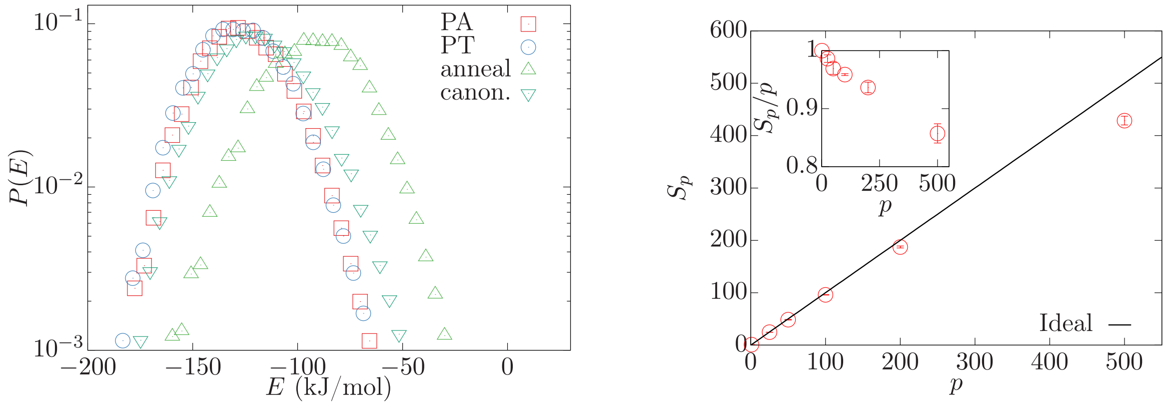

(a) (b)

Figure 12.25: (a) Energy histogram for Met-enkephalin at the lowest temperature ($T = 200$ K) considered for the different methods. (b) Speedup S_p and, in the inset, efficiency S_p/p for different number of CPU cores p.

we adapt Population Annealing [2, 3] to Molecular Dynamics simulations. This method has the advantage that it scales to effectively "arbitrary" number of CPU cores while having comparable performance to Parallel Tempering when using the same computational resources. For a broad range of systems, this opens the door to the world of highly efficient computer simulations on petaflop supercomputers of the present and the exaflop machines of the future. To demonstrate this advantage, we have investigated the penta-peptide Met-enkephalin [4, 5], a system commonly used to probe the performance of novel simulation methods. In Fig. 12.25(a) we show the energy histogram for the lowest temperature considered at $T = 200$ K, where the free-energy barriers are most prominent. Both Population Annealing (PA) and Parallel Tempering (PT) produce energy histograms that are compatible with each other, whereas a single canonical simulation leads to a shifted histogram. Here "anneal" corresponds to an ensemble of independent Simulated Annealing runs. The excellent scaling with the number of CPU cores p is presented in Fig. 12.25(b), where we show the speedup S_p for up to $p = 500$ CPU cores. In the inset, the efficiency S_p/p is shown, indicating a parallel performance of clearly above 80% in this case.

[1] K. Hukushima, K. Nemoto: J. Phys. Soc. Jpn. **65**, 1604 (1996)
[2] Y. Iba: Trans. Jpn. Soc. Artif. Intell. **16**, 279 (2001)
[3] K. Hukushima, Y. Iba: AIP Conf. Proc. **690**, 200 (2003)
[4] H. Christiansen et al.: Phys. Rev. Lett. **122**, 060602 (2019)
[5] H. Christiansen et al.: J. Phys.: Conf. Ser. **1163**, 012074 (2019)

12.24 Framework for programming Monte Carlo simulations (βMC)

M. Marenz, J. Zierenberg*, W. Janke

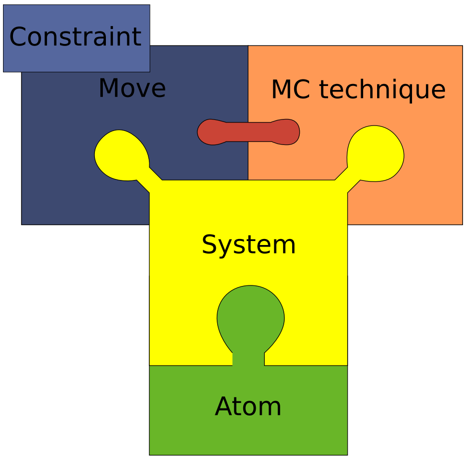

Figure 12.26: The 5 basic building blocks.

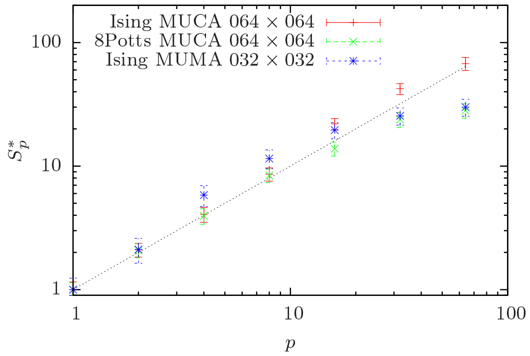

Figure 12.27: Scaling properties of the parallel multicanonical algorithm as a function of the number of processors p.

[*] Max Planck Institute for Dynamics and Self-Organization, Am Fassberg 17,
37077 Göttingen, Germany

Monte Carlo (MC) computer simulations are a very powerful tool for investigating and understanding the thermodynamic behavior of a wide variety of physical systems. These systems range from such simple ones like the Ising or Blume-Capel spin models to complex ones like semiflexible polymers confined in a sphere or proteins interacting with surfaces. In contrast to Molecular Dynamics (MD) simulations, the other important class of algorithm to simulate microscopic systems, MC simulations are not suitable to investigate dynamical properties. On the other hand, the ability of modern MC methods to explore effectively the phase space of physical systems, especially those with a phase transition, makes them a very powerful and indispensable tool.

Another difference to MD simulations is the lack of a widely used program package for generic MC simulations. One reason for this lack is the versatility of modern MC algorithms – there are various different algorithm and many different possibilities to adjust a MC simulation to a specific problem. This was the starting point for the development of our framework for advanced MC algorithms. The aim of the framework is to enable the programmer to implement specific simulations in an easy and efficient way, without the need to implement all the tricky details for every new problem. The framework is implemented in the C++ programming language and is designed such that it separates basics parts of a MC algorithm in separate building blocks. These building blocks can be used by the programmer to implement a specific simulation.

There are 5 basic building blocks as illustrated in Fig. 12.26: The first one is the “system”, which defines the Hamiltonian and the structure of the physical system. This means that the “system” building block encapsulates the energy calculation and the structure of the considered physical problem. For off-lattice system this block contains a smaller subpart, the “atom” block, which encodes the geometry of the system (e.g., boundary conditions). As systems we have implemented so far different kinds of coarse-grained homopolymers, the Lennard-Jones gas, the TIP4P water model, lattice polymers and the Potts model in different dimensions. On top of the “system” are the last two other building blocks, the “move” and the “MC technique”. A “move” defines a single update proposal, propagating the system from the current state to the next one.

Additionally a "constraint" can be added to every "move" in order to simulate efficiently systems with geometrical confinements. The "MC technique" implements the Monte Carlo algorithm itself. At the moment we have implemented various algorithms such as Metropolis MC, parallel tempering, multicanonical MC, multimagnetic MC and the Wang-Landau MC algorithm. One of the most advanced MC algorithms we have implemented is a parallel version of the multicanonical algorithm [1, 2], see Fig. 12.27.

The boundaries between these blocks are well defined, so that one can easily exchange one of them. For example one can use two different algorithm to simulate a specific system without implementing a completely new program. The framework is already in practical use for different studies, for example the investigation of the influence of bending stiffness on a coarse-grained homopolymer, the influence of a spherical confinement to pseudo-phase transitions of homopolymers, and the study of polymer aggregation of several polymers for a large set of parameters (temperature, bending stiffness). Thus, the framework is very useful and has led already to several publications [3–9].

[1] J. Zierenberg et al.: Comput. Phys. Commun. **184**, 1155 (2013)
[2] J. Gross et al.: Comput. Phys. Commun. **224**, 387 (2018)
[3] J. Zierenberg et al.: J. Chem. Phys. **141**, 114908 (2014)
[4] J. Zierenberg, W. Janke: Europhys. Lett. **109**, 28002 (2015)
[5] J. Zierenberg et al: Phys. Rev. E **91**, 032126 (2015)
[6] M. Marenz, W. Janke: Phys. Rev. Lett. **116**, 128301 (2016)
[7] J. Zierenberg et al: Polymers **8**, 333 (2016)
[8] J. Zierenberg et al.: Nat. Commun. **8**, 14546 (2017)
[9] N.G. Fytas et al.: Phys. Rev. E **97**, 040102(R) (2018)

12.25 Funding

Sonderforschungsbereich/Transregio SFB/TRR 102 *Polymers under Multiple Constraints: Restricted and Controlled Molecular Order and Mobility*
W. Janke (Principal Investigator, project B04)
Deutsche Forschungsgemeinschaft (DFG)

Free-Energy Landscapes of Semiflexible Theta-Polymer Aggregation with and without External Force
W. Janke
Deutsche Forschungsgemeinschaft (DFG), Grant No. JA 483/31-1

Stable Knotted Phases in Semiflexible Polymers
W. Janke
Deutsche Forschungsgemeinschaft (DFG), Grant No. JA 483/33-1

COST Action CA17139: EUTOPIA – *European Topology Interdisciplinary Action*
W. Janke (Principal Investigator)

Doctoral College *Statistical Physics of Complex Systems* ($\mathbb{L}^4$)
W. Janke (with B. Berche, Nancy)

Deutsch-Französisches Doktorandenkollegium (DFDK) with "Co-tutelle de Thèse", jointly with Université de Lorraine, Nancy, France, and Coventry University, UK, and National Academy of Sciences of Ukraine, Lviv, Ukraine, as associated partners
Deutsch-Französische Hochschule (DFH-UFA), Grant No. CDFA-02-07

Graduate School *"BuildMoNa": Leipzig School of Natural Sciences – Building with Molecules and Nano-objects*
W. Janke (Principal Investigator)

International Max Planck Research School (IMPRS) *Mathematics in the Sciences*
W. Janke (Scientific Member)
Max Planck Society and Klaus Tschira Foundation

Großgeräteantrag *GPU Cluster*
W. Janke (Principal Investigator, joint application of seven applicants)

12.26 Organizational Duties

Wolfhard Janke

- Director, Institute for Theoretical Physics (ITP), Universität Leipzig
- Director, Naturwissenschaftlich-Theoretisches Zentrum (NTZ), Universität Leipzig
- Member of Department Council ("Fakultätsrat"), Faculty for Physics and Earth Sciences, Universität Leipzig
- Member of the Steering Committee ("Direktorium") of the Graduate Centre *Mathematics/Computer Science and Natural Sciences*, Research Academy Leipzig
- Principal Investigator of the Graduate School "BuildMoNa"
- Scientific Member of the International Max Planck Research School (IMPRS) *Mathematics in the Sciences*
- Principal Investigator of the DFG Sonderforschungsbereich/Transregio SFB/TRR 102 *Polymers under Multiple Constraints: Restricted and Controlled Molecular Order and Mobility*
- Principal Investigator of "Profillinie" *Complex Matter*, Universität Leipzig
- Principal Investigator of "Profillinie" *Mathematical and Computational Sciences*, Universität Leipzig
- Spokesperson of the German-French Graduate College *Statistical Physics of Complex Systems* with Nancy (France), and associated partners in Coventry (England, UK) and Lviv (Ukraine), of the Deutsch-Französische Hochschule (DFH-UFA)
- Scientific Member of the COST Action CA17139: EUTOPIA – *European Topology Interdisciplinary Action*
- *Adjunct Professor* of The University of Georgia, Athens, Georgia, USA
- *International Visiting Professor* of Coventry University, England, UK
- External Member of the Jagiellonian University Graduate School *International Ph.D. Studies in Physics of Complex Systems*, Krakow, Poland
- Permanent Member of the International Advisory Board for the Annual *Conference of the Middle European Cooperation in Statistical Physics (MECO)*

- Organizer (with M. Weigel, Coventry University, UK) of the CECAM Workshop *New Methods in Monte Carlo Simulations: Parallel, Adaptive, Irreversible*, CECAM-HQ-EPFL, Lausanne, Switzerland, 02.–04. September 2019
- Organizer of the Workshop *CompPhys19* – 20th International NTZ Workshop on *New Developments in Computational Physics*, ITP, Universität Leipzig, 28.–30. November 2019
- Organizer of the Workshop *CompPhys20* – 21th International NTZ Workshop on *New Developments in Computational Physics*, ITP, Universität Leipzig, 03.–05. December 2020
- Editor "Computational Physics", *Central European Journal of Physics*, Krakow, Poland
- Member of Editorial Board, *Condens. Matter Phys.*, Lviv, Ukraine
- Member of the Editorial Board, Topic Editor, *Polymers*, MPDI, Basel, Switzerland
- Member of Editorial Board, *e-books Programme*, IOP Publishing Limited
- External Reviewer for Deutsche Forschungsgemeinschaft (DFG); Humboldt-Stiftung (AvH); Studienstiftung des deutschen Volkes; Fond zur Förderung der wissenschaftlichen Forschung (FWF), Österreich; The Royal Society, UK; The Engineering and Physical Sciences Research Council (EPSRC), UK; Israel Science Foundation, Israel; National Science Foundation (NSF), USA; Natural Sciences and Engineering Research Council of Canada (NSERC), Canada; The Jeffress Memorial Trust, Bank of America, Virginia, USA; Universität Mainz, Germany; The University of Warwick, England, UK; Coventry University, England, UK; CECAM, Lausanne, Switzerland
- Referee for Physical Review Letters, Physical Review B, Physical Review E, Journal of Chemical Physics, Europhysics Letters, Physics Letters A, Physics Letters B, The European Physical Journal B, Physica A, Proceedings of the Royal Physical Society, Journal of Physics A, Computer Physics Communications, JSTAT, Canadian Journal of Physics, Condens. Matter Phys., PLOS ONE, New Journal of Physics, International Journal of Modern Physics C

12.27 External Cooperations

Academic

- Institute of Physics, Jagiellonian University, Kraków, Poland
  Prof. Dr. Piotr Białas, Dr. Leszek Bogacz, Prof. Dr. Zdzisław Burda
- CEA/Saclay, Service de Physique Théorique, France
  Dr. Alain Billoire
- Institut für Physik, Universität Mainz, Germany
  Prof. Dr. Kurt Binder, Andreas Nußbaumer, Prof. Dr. Friderike Schmid
- Institut für Theoretische Physik, Universität Heidelberg, Germany
  Dr. Elmar Bittner
- Laboratoire de Physique des Matériaux (UMR CNRS No 7556), Université de Lorraine, Nancy, France
  Prof. Dr. Bertrand Berche, Dr. Christophe Chatelain, Dr. Olivier Collet, Prof. Dr. Malte Henkel, Prof. Dr. Dragi Karevski

- Groupe de Physique des Matériaux (UMR CNRS No 6634), Université de Rouen, France
  Dr. Pierre-Emmanuel Berche
- SUPA, School of Physics and Astronomy, University of Edinburgh, Scotland, UK
  Dr. Richard A. Blythe, Prof. Dr. Martin R. Evans, Dr. Bartłomiej Wacław
- P.J. Šafárik University, Košice, Slovak Republic
  Dr. Michal Borovský
- Istituto Nazionale di Fisica Nucleare, Sezione di Milano-Bicocca, Milano, Italy
  Prof. Dr. Pablo Butera
- Institute of Physical Chemistry and Electrochemistry, Leibniz Universität Hannover, Germany
  Prof. Dr. Jürgen Caro
- Applied Mathematics Research Centre, Coventry University, England, UK
  PD Dr. Christian von Ferber, Dr. Nikolaos G. Fytas, Prof. Dr. Ralph Kenna, Dr. Thierry Platini, Dr. Martin Weigel
- Jülich Supercomputing Centre (JSC), Forschungszentrum Jülich, Germany
  Prof. Dr. Peter Grassberger
- IAC-1, Universität Stuttgart, Germany
  Prof. Dr. Rudolf Hilfer, Prof. Dr. Christian Holm
- Max Planck Institute for Polymer Research, Mainz, Germany
  Dr. Hsiao-Ping Hsu, Prof. Dr. Kurt Kremer
- Complex Systems Division, Department of Theoretical Physics, Lunds Universitet, Lund, Sweden
  Prof. Dr. Anders Irbäck
- Department of Mathematics and the Maxwell Institute for Mathematical Sciences, Heriot-Watt University, Edinburgh, Scotland, UK
  Prof. Dr. Desmond A. Johnston
- Inst. für Theoretische Physik, FU Berlin, Germany
  Prof. Dr. Hagen Kleinert
- Department of Physics, University of Athens, Zografou, Greece
  Prof. Dr. Anastasios Malakis
- Atominstitut, TU Wien, Austria
  Prof. Dr. Harald Markum
- Jacobs Universität Bremen, Germany
  Prof. Dr. Hildegard Meyer-Ortmanns, Darka Labavić
- Institute of Physics, Polish Academy of Sciences, Warsaw, Poland
  Dr. Panagiotis E. Theodorakis
- Applied Mathematics, Universitat Pompeu Fabra, Barcelona, Spain
  Prof. Dr. Ramon Villanova
- CERN (PH-SFT), Geneva, Switzerland
  Dr. Sandro Wenzel

- Department of Engineering of Physics, Ankara University, Ankara, Turkey
  Prof. Dr. Handan Arkın-Olgar, Mustafa Bilsel, Dogukan Hazar Özbey, Buket Taşdizen
- Dept. of Physics, Hacettepe University, Ankara, Turkey
  Prof. Dr. Tarik Çelik, Gökhan Gökoğlu
- Dept. of Physics Engineering, Hacettepe University, Ankara, Turkey
  Prof. Dr. Fatih Yaşar
- Institute for Condensed Matter Physics, National Academy of Sciences, Lviv, Ukraine
  Dr. Viktoria Blavatska, Prof. Dr. Yurij Holovatch
- Yerevan Physics Institute, Yerevan, Armenia
  Prof. Dr. David B. Saakian
- Alikhanyan National Science Laboratory, Yerevan, Armenia
  Prof. Dr. Nerses Ananikyan, Dr. Nikolay Izmailyan
- Landau Institute for Theoretical Physics, Chernogolovka, Russia
  Dr. Lev Yu. Barash, Prof. Dr. Lev N. Shchur
- National Research University Higher School of Economics, Moscow, Russia
  Prof. Dr. Evgeni Burovski, Maria Guskova
- Center for Simulational Physics, The University of Georgia, Athens, USA
  Prof. Dr. Michael Bachmann, Prof. Dr. David P. Landau
- Dept. of Physics, Florida State University, Tallahassee, USA
  Prof. Dr. Bernd A. Berg
- Dept. of Chemistry and Biochemistry, University of Oklahoma, Norman, USA
  Prof. Dr. Ulrich H.E. Hansmann
- Los Alamos National Laboratory, Los Alamos, USA
  Dr. Christoph Junghans
- Dept. of Physics and Astronomy, Texas A&M, College Station, USA
  Prof. Dr. Helmut G. Katzgraber
- Dept. of Physics, Virginia Tech, Blacksburg, USA
  Prof. Dr. Michel Pleimling, Prof. Dr. Royce K.P. Zia
- Physics Department, Carnegie Mellon University, Pittsburgh, USA
  Prof. Dr. Robert H. Swendsen
- University of North Georgia, Dahlonega, USA
  Dr. Thomas Vogel
- Banaras Hindu University, Varanasi, India
  Prof. Dr. Sanjay Kumar
- Jawaharlal Nehru Centre for Advanced Scientific Research (JNCASR), Jakkur, India
  Prof. Dr. Subir K. Das
- School of Physical Sciences, Jawaharlal Nehru University, New Delhi, India
  Manoj Kumar, Prof. Dr. Sanjay Puri
- Department of Physics, Indian Institute of Technology, Hauz Khas, New Delhi, India
  Prof. Dr. Varsha Banerjee

- Computational Chemistry Unit Cell (CCUC), Department of Chemistry, Chulalongkorn University, Bangkok, Thailand
  Prof. Dr. Supot Hannongbua, Dr. Oraphan Saengsawang
- Metallurgy and Materials Science Research Institute (MMRI), Chulalongkorn University, Bangkok, Thailand
  Prof. Dr. Rungroj Chanajaree
- Department of Chemistry, Faculty of Science, Ramkhamhaeng University, Bangkok, Thailand
  Dr. Tatiya Chokbunpiam
- Faculty of Applied Science and Engineering, Khon Kaen University, Nong Khai Campus, Nong Khai, Thailand
  Prof. Dr. Tawun Remsungnen
- Laboratory of Statistical and Computational Physics, Institute of Physics, Academia Sinica, Nankang, Taipei, Taiwan
  Prof. Dr. Chin-Kun Hu
- Zhejiang Institute of Modern Physics, Zhejiang University, Hangzhou, P.R. China
  Prof. Dr. He-Ping Ying, Prof. Dr. Bo Zheng
- The University of Tokyo, Tokyo, Japan
  Prof. Dr. Nobuyasu Ito
- Nagoya University, Nagoya, Japan
  Dr. Tetsuro Nagai, Prof. Dr. Yuko Okamoto

12.28 Publications

Journals

E. Burovski, W. Janke, M. Guskova, L. Shchur: *Acceptance Rate is a Thermodynamic Function in Local Monte Carlo Algorithms (Editors' Suggestion)*, Phys. Rev. E **100**, 063303-1–8 (2019)

T. Chokbunpiam, R. Chanajaree, J. Caro, W. Janke, T. Remsungnen, S. Hannongbua, S. Fritzsche: *Separation of Nitrogen Dioxide from the Gas Mixture with Nitrogen by Use of ZIF materials; Computer Simulation Studies*, Comput. Mater. Sci. **168**, 246–252 (2019)

H. Christiansen, S. Majumder, W. Janke: *Phase Ordering Kinetics of the Long-Range Ising Model*, Phys. Rev. E **99**, 011301(R)-1–5 (2019)

H. Christiansen, M. Weigel, W. Janke: *Accelerating Molecular Dynamics Simulations with Population Annealing*, Phys. Rev. Lett. **122**, 060602-1–5 (2019)

H. Christiansen, M. Weigel, W. Janke: *Population Annealing Molecular Dynamics with Adaptive Temperature Steps*, J. Phys.: Conf. Ser. **1163**, 012074-1–6 (2019)

W. Janke, H. Christiansen, S. Majumder: *Coarsening in the Long-Range Ising Model: Metropolis versus Glauber Criterion*, Invited Plenary Talk at the International Conference on *Computer Simulation in Physics and beyond (CSP2018)*, 24–27 September 2018, Moscow, Russia, J. Phys.: Conf. Ser. **1163**, 012002-1–10 (2019)

S. Majumder, H. Christiansen, W. Janke: *Dissipative Dynamics of a Single Polymer in Solution: A Lowe-Andersen Approach*, J. Phys.: Conf. Ser. **1163**, 012072-1–6 (2019)

S. Majumder, U.H.E. Hansmann, W. Janke: *Pearl-Necklace-Like Local Ordering Drives Polypeptide Collapse*, Macromolecules **52**, 5491–5498 (2019)

S. Roy, A. Bera, S. Majumder, S.K. Das: *Aging Phenomena During Phase Separation in Fluids: Decay of Autocorrelation for Vapor-Liquid Transitions*, Soft Matter **15**, 4743–4750 (2019)

S. Schnabel, W. Janke: *Distribution of Metastable States of Spin Glasses*, in: *Computer Simulation Studies in Condensed-Matter Physics XXXI*, eds. D.P. Landau, M. Bachmann, S.P. Lewis, H.-B. Schüttler, J. Phys.: Conf. Ser. **1252**, 012001-1–6 (2019)

L. Shchur, L. Barash, M. Weigel, W. Janke: *Population Annealing and Large Scale Simulations in Statistical Mechanics*, Communications in Computer and Information Science (CCIS) **965**, 354–366 (2019)

in press

H. Christiansen, S. Majumder, M. Henkel, W. Janke: *Aging in the Long-Range Ising Model*, Phys. Rev. Lett. **125**, 180601-1–7 (2020)

S.K. Das, K. Das, N. Vadakkayil, S. Chakraborty, S. Paul: *Initial Correlation Dependence of Aging in Phase Separating Solid Binary Mixtures and Ordering Ferromagnets*, J. Phys.: Cond. Mat. **32**, 184005-1–7 (2020)

S. Fritzsche, T. Chokbunpiam, J. Caro, S. Hannongbua, W. Janke, T. Remsungnen: *Combined Adsorption and Reaction in the Ternary Mixture N_2, N_2O_4, NO_2 on MIL-127 Examined by Computer Simulations*, ACS Omega **5**, 13023–13033 (2020)

S. Kazmin, W. Janke: *Critical Exponent ν of the Ising Model in Three Dimensions with Long-Range Correlated Site Disorder Analyzed with Monte Carlo Techniques*, Phys. Rev. B **102**, 174206-1–13 (2020)

R. Kumar, J. Gross, W. Janke, M. Weigel: *Massively Parallel Simulations for Disordered Systems*, contribution to Topical Issue on *Recent Advances in the Theory of Disordered Systems*, Eur. Phys. J. B **93**, 79-1–13 (2020)

S. Majumder, H. Christiansen, W. Janke: *Understanding Nonequilibrium Scaling Laws Governing Collapse of a Polymer*, Invited Colloquium, Eur. Phys. J. B **93**, 142-1–19 (2020)

F. Müller, S. Schnabel, W. Janke: *Nonflat Histogram Techniques for Spin Glasses*, Phys. Rev. E **102**, 053303-1–8 (2020)

S. Schnabel, W. Janke: *Counting Metastable States of Ising Spin Glasses on Hypercubic Lattices*, contribution to Topical Issue on *Recent Advances in the Theory of Disordered Systems*, Eur. Phys. J. B **93**, 53-1–7 (2020)

S. Schnabel, W. Janke: *Polymer Simulation by Means of Tree Data-Structures and a Parsimonious Metropolis Algorithm*, Comput. Phys. Commun. **256**, 107414-1–9 (2020)

W. Janke, S. Majumder, S.K. Das: *Domain Coarsening in the Potts Model Described by Universal Finite-Size Scaling Function*, Leipzig/Bangalore preprint (March 2019), to appear in the Proceedings *Computer Simulation Studies in Condensed-Matter Physics XXXII*, eds. D.P. Landau, M. Bachmann, S.P. Lewis, and H.-B. Schüttler, J. Phys.: Conf. Ser. (in print)

S. Paul, S.K. Das: *Dependence of Cluster Growth on Coefficient of Restitution in a Cooling Granular Fluid*, to appear in Bulletin of Materials Science (2020), in print

Talks

H. Christiansen: *Accelerating Molecular Dynamics Simulations with Population Annealing*, DPG Frühjahrstagung 2019, Universität Regensburg, Germany, 31. March – 05. April 2019

H. Christiansen: *Coarsening and Aging in the Long-Range Ising Model*, CECAM Workshop *New Methods in Monte Carlo Simulations: Parallel, Adaptive, Irreversible*, Lausanne, Switzerland, 02.–04. September 2019

H. Christiansen: *Tuning Interaction in Long-Range Models Changes Dynamical Scaling During Aging*, 20th International NTZ-Workshop on *New Developments in Computational Physics – CompPhys19*, Universität Leipzig, Germany, 28.–30. November 2019

W. Janke: *Universal Finite-Size Scaling Function for Phase Separation Kinetics in Multicomponent Mixtures*, 32nd Annual CSP Workshop on *Recent Developments in Computer Simulation Studies in Condensed Matter Physics*, The University of Georgia, Athens, Georgia, USA, 18.–22. February 2019

W. Janke: *Coarsening Dynamics of the Long-Range Ising Model*, DPG Frühjahrstagung 2019, Universität Regensburg, Germany, 31. March – 05 April 2019

W. Janke: *Accelerating Molecular Dynamics Simulations with Population Annealing*, Conference of the Middle European Cooperation in Statistical Physics – MECO44, Kloster Seeon, Germany, 01.–03. May 2019

W. Janke: *Accelerating Molecular Dynamics Simulations of Peptide Folding with Population Annealing*, invited talk, XXXI IUPAP Conference on Computational Physics (CCP2019), Chinese University of Hong Kong, 28. July – 01. August 2019

W. Janke: *Quantum Monte Carlo Methods*, three invited lectures, Bad Honnef Physics School *Methods of Path Integration in Modern Physics*, Physikzentrum Bad Honnef, Germany, 25.–31. August 2019

W. Janke: *Accelerating Molecular Dynamics Through Populations*, CECAM Workshop *New Methods in Monte Carlo Simulations: Parallel, Adaptive, Irreversible*, CECAM-HQ, Lausanne, Switzerland, 02.–04. September 2019

S. Kazmin: *Critical Exponent* ν *of the Ising Model in Three Dimensions with Long-Range Correlated Disorder*, 20th International NTZ-Workshop on *New Developments in Computational Physics – CompPhys19*, Universität Leipzig, Germany, 28.–30. November 2019

S. Majumder, S.K. Das, W. Janke: *Universal Finite-Size Scaling for Kinetics of Phase Separation in Multicomponent Mixtures*, DPG Frühjahrstagung 2019, Universität Regensburg, Germany, 31. March–5. April 2019

S. Paul: *Collapse Dynamics of Polymers with Vicsek-like Activity*, DPG Frühjahrstagung 2019, Universität Regensburg, Germany, 31. March – 05 April 2019

S. Paul: *Collapse Dynamics of a Flexible Polymer with Active Beads*, 20th International NTZ-Workshop on *New Developments in Computational Physics – CompPhys19*, Universität Leipzig, Germany, 28.–30. November 2019

S. Schnabel, W. Janke: *Simulation of a Large Polymer with Untruncated Interaction near the Collapse*, DPG Frühjahrstagung 2019, Universität Regensburg, Germany, 31. March – 04. April 2019

S. Schnabel, W. Janke: *Simulation of a Large Polymer with Untruncated Interaction near the Collapse*, CECAM Workshop *New Methods in Monte Carlo Simulations: Parallel, Adaptive, Irreversible*, CECAM-HQ, Lausanne, Switzerland, 02.–04. September 2019

S. Schnabel, W. Janke: *Collapse Transition of a Long Polymer with and without Periodic Boundary Conditions*, 20th International NTZ-Workshop on *New Developments in Computational Physics – CompPhys19*, Universität Leipzig, Germany, 28.–30. November 2019

Posters

H. Christiansen, M. Weigel, W. Janke: *Accelerating Molecular Dynamics Simulations with Population Annealing*, Soft Matter Day 2019, Universität Leipzig, Germany, 05. July 2019

S. Kazmin: *Critical Exponent* ν *of the Ising Model in Three Dimensions with Long-Range Correlated Disorder*, DPG Frühjahrstagung 2019, Universität Regensburg, Germany, 31. March – 05. April 2019

S. Majumder, U. Hansmann, W. Janke: *Pearl-Necklace-Like Local Ordering Drives Polypeptide Collapse*, Conference of the Middle European Cooperation in Statistical Physics – MECO44, Kloster Seeon, Germany, 01.–03. May 2019

S. Majumder, U. Hansmann, W. Janke: *Pearl-Necklace-Like Local Ordering Drives Polypeptide Collapse*, 20th International NTZ-Workshop on *New Developments in Computational Physics–CompPhys19*, Universitaät Leipzig, Germany, 28.–30. November 2019

S. Paul, S. Majumder, S.K. Das, W. Janke: *Collapse Dynamics of a Flexible Polymer with Active Beads*, Conference of the Middle European Cooperation in Statistical Physics – MECO44, Kloster Seeon, Germany, 01.–03. May 2019

12.29 Graduations

Doctorate

- Momchil Ivanov
  Monte Carlo Simulations of Thiophene and Polythiophene Chains of Various Lengths in Vacuum and in Contact with Substrates
  28. May 2019

Master

- Tobias Weiss
  Simulation des 2d Ising Modells auf der GPU und Anwendung auf ein Interpolationsmodell
  19. November 2019

Bachelor

- Denis Gessert
  Anomalous Zero-Temperature Phase Ordering Dynamics of the 3D Ising Model with a GPU Implementation
  11. April 2019
- Alex Panchot
  Non-Flat Wang-Landau Algorithm
  25. June 2019
- Hoang Linh Nguyen
  Population Annealing Monte-Carlo in Spin Models – Investigating the Effect of Different Resampling Methods on the 2D Ising Model
  03. September 2019
- Max Staats
  Influence of the Cut-Off Range on Phase Ordering Kinetics in the Long-Range Ising Model
  26. September 2019
- Cameron Perot
  Phase Transition Continuity Dependence on Edge Evaluation and Acceptance
  14. October 2019

12.30 Guests

- Prof. Dr. Subir K. Das
  Jawaharlal Nehru Centre for Advanced Scientific Research, Bangalore, India

DFH-UFA Colloquium (23. May 2019)
How Does a Coarsening Ferromagnet Lose the Memory of its Origin?
22.–24. May 2019

- Piotr Kuterba
  Jagiellonian University, Krakow, Poland
  Research Stay
  Seminar (13. June 2019)
  Field Theoretical and Simulation Approach to Dilute Solutions of Ring Polymers with Excluded-Volume Interaction in a Slit Geometry with Mixed Boundary Conditions
  Seminar (27. June 2019)
  Molecular Dynamics Simulations of a Single Polymer Chain Confined in a Slit Between one Attractive and one Repulsive Wall
  01.–30. June 2019
- Jude Ann Vishnu
  Mohali, India
  Internship
  Seminar (04. July 2019)
  MC Simulation of q-States Potts Model with Invisible States on a 2d Lattice for Studying Nonequilibrium Aspects
  03. June – 31. July 2019
- Dr. Antonio Astillero
  Universidad de Extremadur, Spain
  Off-Equilibrium Computation of the Dynamic Critical Exponent of the Three-Dimensional Heisenberg Model
  27. November – 01. December 2019
- Kurt Binder
  Johannes-Gutenberg-Universität Mainz, Germany
  Physik-Kolloquium (28. November 2019)
  Statistical Mechanics and Phase Transitions of Semiflexible Polymers
  27.–29. November 2019
- Dr. Elmar Bittner
  Universität Heidelberg, Germany
  28.–29. November 2019
- Saikat Chakraborty
  Johannes-Gutenberg-Universität Mainz, Germany
  Steric Effects and Hydrophobic Interactions determine One-Dimensional Self-Assembly
  27.–30. November 2019
- Tatiya Chokbunpiam
  Department of Chemistry and Center of Excellence for Innovation in Chemistry, Faculty of Science, Ramkhamhaeng University, Bangkok, Thailand
  Extraordinary Adsorption/Reaction Selectivity of NO_x from N_2 by Combined Adsorption and Reaction on MIL-127
  27.–30. November 2019
- Prof. Dr. Ulrich H.E. Hansmann
  University of Oklahoma, Norman, OK, USA

Structural Transitions in Protein Folding and Amyloid Formation
26.–29. November 2019

- Prof. Dr. Alexander Hartmann
  Universität Oldenburg, Germany
  Large-Deviation Simulation of Height Distribution for the KPZ Equation: Dependence on Initial Conditions and Morphology of Extreme Configurations
  27.–29. November 2019
- Dr. Martin Hasenbusch
  Universität Heidelberg, Germany
  Monte Carlo Study of an Improved Clock Model in Three Dimensions
  27.–30. November 2019
- Prof. Dr. Malte Henkel
  Université de Lorraine Nancy, France
  Meta-Conformal Invariance in Directed Kinetic Spin Models
  27.–29. November 2019
- Dr. Hsiao-Ping Hsu
  MPI Polymer Research, Mainz, Germany
  New Development of a Coarse-Grained Model for Studying the Glass Transition of Polymer Melts
  27.–29. November 2019
- Dr. Fred Hucht
  Universität Duisburg-Essen, Germany
  Bond-Flip Monte Carlo Based on Exact Results for the Square-Lattice Ising Model
  27.–30. November 2019
- Prof. Dr. Ferenc Igloi
  Wigner Research Centre, Budapest, Hungary
  Reentrant Random Quantum Ising Antiferromagnet
  27.–30. November 2019
- Prof. Dr. Desmond A. Johnston
  Heriot-Watt University, Edinburgh, Scotland, UK
  Lattice SUSY and the DiSSEP
  27. November – 01. December 2019
- Dr. Anja Kuhnhold
  Albert-Ludwigs-Universität Freiburg, Germany
  Monte Carlo Simulations of Chiral Colloidal Membranes
  27.–30. November 2019
- Manoj Kumar
  Coventry University, England, UK
  Critical Behavior and Approximate Ground States in the Random-Field Potts Model via Graph Cuts
  27.–30. November 2019
- Dr. Eunsang Lee
  Martin-Luther Universität Halle, Germany

  Additional Topological Effect Imposed by Ring-shaped Aggregates in Supramolecular Polymer Melts
  28.–29. November 2019

- Prof. Dr. Arnulf Möbius
  IFW Dresden, Germany
  28.–29. November 2019
- Dr. Gergö Roósz
  TU Dresden, Germany
  Interacting Majorana Modes on Surfaces of Noncentrosymmetric Superconductors
  28.–30. November 2019
- Walter Selke
  RWTH Aachen, Germany
  28.–29. November 2019
- Dr. Timur Shakirov
  Martin-Luther Universität Halle, Germany
  Crystallisation in Melts of Short, Semi-Flexible Hard-Sphere Polymer Chains: The Role of the Non-Bonded Interaction Range
  28.–29. November 2019
- Prof. Dr. Zoryana E. Usatenko
  Cracow University of Technology, Krakow, Poland
  Ring Polymer Chains in Confined Geometries
  27.–30. November 2019
- Dimitrios Voliotis
  IFSC, University of Sao Paulo, Brazil
  Multifractality in Aperiodic Quantum Spin Chains
  27.–29. November 2019